LHC signature of supersymmetric models with non-universal sfermion masses

JHEP10(2009)005

(http://iopscience.iop.org/1126-6708/2009/10/005)

Published by IOP Publishing for SISSA
Received: *July 29, 2009*
Revised: *August 30, 2009*
Accepted: *September 8, 2009*
Published: *October 2, 2009*

LHC signature of supersymmetric models with non-universal sfermion masses

Sung-Gi Kim,[a] **Nobuhiro Maekawa,**[b] **Keiko I. Nagao,**[b] **Mihoko M. Nojiri**[c,d] **and Kazuki Sakurai**[e]

[a] *Department of Physics, Tohoku University, Sendai 980-8578, Japan*
[b] *Department of Physics, Nagoya University, Nagoya 464-8602, Japan*
[c] *KEK Theory Center, IPNS, KEK, The Graduate University for Advanced Studies (Sokendai), 1-1 Oho, Tsukuba, 305-0801, Japan*
[d] *IPMU, Tokyo University, Kashiwa, Chiba, 277-8568, Japan*
[e] *KEK Theory Center, IPNS, KEK, 1-1 Oho, Tsukuba, 305-0801, Japan*
E-mail: kimsg@indiana.edu, maekawa@eken.phys.nagoya-u.ac.jp, nagao@eken.phys.nagoya-u.ac.jp, nojiri@post.kek.jp, ks563@cam.ac.uk

Abstract: We study the LHC signature of the minimal supersymmetric standard model with non-universal sfermion masses. In the model, soft masses of gauginos and the 3rd generation of **10** of SU(5) are around the weak scale, while other sfermion soft mass is universal and around a few TeV. Such sfermion mass spectrum is motivated not only from flavor, CP and naturalness constraints but also from E_6 grand unified model with non-Abelian horizontal (flavor) symmetry. The characteristic signature of the model at the LHC is the dominance of the events with 4 b partons in the final state together with high rate of mildly boosted top quark arising from gluino decay. The prominent high p_T jet also arises from squark decay. We show it is possible to find the characteristic signature in the early stage of the LHC. The discrimination of our scenario from some CMSSM model points with similar signature may be possible with large integrated luminosity. The result of sparticle mass measurement using exclusive channel with the help of hemisphere analysis, and inclusive measurement of gluino and squark masses using M_{T2} and $M_{T2}^{\min}$ in some representative model points are presented.

Keywords: Supersymmetry Phenomenology

ArXiv ePrint: 0907.4234

doi:10.1088/1126-6708/2009/10/005

JHEP10(2009)005

Contents

JHEP10(2009)005

1 Introduction

Supersymmetry (SUSY) is one of the most promising candidates for physics beyond the Standard Model (SM). The minimal supersymmetric standard model (MSSM) has some attractive features, for instance improvement of the gauge coupling unification, the radiative electroweak symmetry breaking, and providing a dark matter candidate as the lightest superparticle (LSP) [1–3]. Moreover, one of the most attractive features of the MSSM is the stabilization of the weak scale in the case that the SUSY breaking parameters and the higgsino mass parameter (μ) are around the weak scale. The signatures of the supersymmetry may be discovered and some properties of the MSSM will be revealed at ATLAS and CMS experiments at the CERN Large Hadron Collider (LHC). The LHC signatures of various SUSY models, such as minimal supergravity (mSUGRA) model [4–7], gauge mediated SUSY breaking (GMSB) model [8–10], anomaly mediated SUSY breaking (AMSB) model [11–15], mixed modulas anomaly mediation (MMAM) model [16, 17], have been studied.

The sparticle mass measurement is an important physics target at the LHC. Various methods have been developed for sparticle mass determination from event kinematics [4-7, 18-35]. Endpoint methods of the various leptonic exclusive channels is known to be very successful [4–7, 18, 19]. By combining the measured endpoints of the invariant mass distributions of the jets and leptons from relatively clean and long cascade decay channels involving neutralinos ($\widetilde{\chi}_i^0$) and sleptons ($\widetilde{l}$), one can determine not only the masses of the squark and gluino, but also the masses of neutralinos and sleptons arising from their cascade decays. Recently, progress has been made in the use of M_{T2} distributions for the sparticle mass measurement [27–35]. It has been pointed out that the endpoint of the M_{T2} distributions as a function of the test LSP mass (χ) may exhibit a kink, which indicates the initially produced sparticle mass and the true LSP mass simultaneously [29–31]. Moreover if we define the M_{T2} and the sub-system M_{T2} [33, 34] inclusively, we can roughly measure the squark and gluino masses even in the very early stage at the LHC [32, 33, 36].

The purpose of this paper is investigating the LHC signature of SUSY models with non-universal sfermion masses. Most of the SUSY models that have been studied so far have universality of sfermion soft masses in the flavor space except for some literature [37–39]. Introduction of the sfermion non-universality may induce unacceptably large flavor changing neutral currents (FCNCs) and electric dipole moments (EDMs) [40–43]. However, the sfermion non-universality may be partially introduced for the 3rd generation sfermions because constraints from the 3rd generation FCNCs are not so severe [44–46] (See also refs. [47–49]). If soft masses of gluino and right and left-handed stops are around the weak scale while the other sfermion masses are around a few TeV, some of FCNC and EDM constraints are relaxed with keeping weak scale stabilization. In grand unified theories (GUTs) such as SU(5) GUT, both the left and right-handed stops are involved in the 3rd generation of **10**-plet of SU(5). In this paper, we consider a minimal non-univeral models in which only the 3rd generation sfermions involved in **10** have a different soft mass (m_{30}) from the other universal soft sfermion mass (m_0) at the cutoff scale. The non-universal sfermion mass scenario is motivated both on phenomenological and theoretical grounds. There are models that predict the non-universal structure adopted in this paper along with realistic fermion masses and mixing matrices [50, 51].

This paper is organized as follows. In section 2, we introduce a non-universal sfermion mass scenario and explain motivations. We identify the motivated region of parameter space from some phenomenological constraints. In section 3, we investigate the LHC signature at some representative model points. The charactaristic signature of the model is the 4 b partons in the final state and mildly boosted top quark with high rate for gluino gluino production. The prominent high p_T jet also arises for squark gluino co-production. We demonstrate that it is possible to find the characteristic signature of the model through particle level Monte Carlo Simulation with detector smearing. In section 4, we search constrained MSSM (CMSSM) parameter space [52], where all scalar fields have common SUSY breaking mass at the cutoff scale, and find a model point whose signature is similar to that of our scenario. We propose a key measurement to discriminate our scenario from the CMSSM model point. In section 5, we discuss sparticle mass measurement in our scenario. We study leptonic exclusive analysis, the top reconstruction from gluino decay, and measurement of

JHEP10(2009)005

the tb endpoint. We also study inclusive M_{T2} and $M_{T2}^{\rm min}$ distributions [32, 33, 36] and demonstrate that gluino and the first two generation squark masses can be measured in a stage of the LHC such as $\int \mathcal{L}dt = 5 - 20$ fb^{-1}. Section 6 is devoted to the conclusion.

2 Modified universal sfermion mass scenario

In supersymmetric models there is no quadratic divergence in the Higgs sector. Therefore the naturalness problem in the SM is significantly relaxed. However the supersymmetry is softly broken and the scale of the quantum correction to the Higgs mass is of the order of the soft SUSY breaking parameters. If the SUSY breaking scale is much lager than the weak scale, unnatural tuning among the soft masses and higgsino mass, μ, is required.

Let us look this issue more closely. In the MSSM, the condition for the electroweak symmetry breaking (EWSB) is given as

$$\frac{m_Z^2}{2} = -|\mu|^2 - m_{H_u}^2(\Lambda) - \Delta m_{H_u}^2 + \mathcal{O}\left(\frac{m_{H_{u,d}}^2}{\tan^2\beta}\right), \tag{2.1}$$

where $m_{H_u}^2(\Lambda)$ is a soft mass of the up-type Higgs boson at the cutoff scale Λ, and $\Delta m_{H_u}^2$ is a quantum correction to the $m_{H_u}^2$ at the weak scale, which is roughly given as

$$\Delta m_{H_u}^2 \sim -\frac{6|Y_t|^2}{(4\pi)^2} m_{\tilde{t}}^2 \ln\left(\frac{\Lambda^2}{m_{\tilde{t}}^2}\right), \tag{2.2}$$

where Y_t is the top Yukawa coupling and $m_{\tilde{t}}$ is the averaged stop mass. The $\Delta m_{H_u}^2$ is large if $m_{\tilde{t}}$ is much larger than the weak scale. In that case, a relatively large cancellation is required among the terms in the right hand side of eq. (2.1).

Unlike stop masses, the other squark and slepton masses do not affect the Higgs potetial because their Yukawa couplings are small unless the bottom Yukawa coupling is as large as the top Yukawa coupling. As long as both left and right-handed stop masses are around the weak scale, we can take their masses much larger than the weak scale. In SU(5) GUT, two stops are unified into a single **10**-plet field at the GUT scale. We consider a model in which a soft mass of the 3rd generation of **10** (**10**$_3$) is independent of the other universal sfermion soft masses at the GUT scale. We parameterize sfermion soft mass matrices at the cutoff scale as follows:

$$m_{\mathbf{10}}^2 = \begin{pmatrix} m_0^2 & & \\ & m_0^2 & \\ & & m_{30}^2 \end{pmatrix}, \qquad m_{\overline{\mathbf{5}}}^2 = \begin{pmatrix} m_0^2 & & \\ & m_0^2 & \\ & & m_0^2 \end{pmatrix}. \tag{2.3}$$

Here, $\mathbf{10} = (Q, U^c, E^c)$, $\overline{\mathbf{5}} = (D^c, L)$. In this paper, we take the cutoff Λ to be the unification scale of the three gauge couplings ($\Lambda \simeq 2 \times 10^{16}$ GeV).

In the super-CKM basis, sfermion mass matrices for **10** sector are given as $m_{\tilde{f}}^2 = V_f^\dagger m_{\mathbf{10}}^2 V_f$ ($f = u_L, d_L, u_R, e_R$) at the cutoffs scale. Here V_f are unitary matrices that diagonalize the Yukawa matrices as $V_{u_L}^T Y_u V_{u_R}^* = Y_u^{\rm diag}$. The mixing induced by V_f should be sufficiently small to avoid large FCNCs. Thus in addition to eq. (2.3), we assume [47–49],

$$(V_{u_L})_{ij},\ (V_{d_L})_{ij},\ (V_{u_R})_{ij},\ (V_{e_R})_{ij} \lesssim (V_{\rm CKM})_{ij}, \qquad (i \neq j). \tag{2.4}$$

In E_6 SUSY GUT models with SU(2) $\times$ U(1) horizontal symmetry H, eqs. (2.3) and (2.4) are derived along with realistic fermion masses and mixing matrices [50, 51]. In the models, all the $\overline{\mathbf{5}}$-plets of three families and the first two generations of $\mathbf{10}$-plets ($\mathbf{10}_1$ and $\mathbf{10}_2$) are involved in a SU(2)$_H$ doublet, $\Psi(\mathbf{27},\mathbf{2})_a = (\Psi_1, \Psi_2)$, while $\mathbf{10}_3$ and MSSM Higgs fields are involved in SU(2)$_H$ singlets, $\Psi(\mathbf{27},\mathbf{1})_3$ and $\Phi(\mathbf{27},\mathbf{1})$, respectively.[1] The Yukawa terms for $\Psi(\mathbf{27},\mathbf{2})_a$ are forbidden by SUSY and the horizontal symmetry of the superpotential. On the other hand, a term $W \ni \Psi(\mathbf{27},\mathbf{1})_3\Psi(\mathbf{27},\mathbf{1})_3\Phi(\mathbf{27},\mathbf{1})$ is allowed. Thus, the Yukawa coupling for $\mathbf{10}_3$ can be of order one, which is identified as the top Yukawa coupling.

Other Yukawa couplings arise though the higher dimensional operators after breaking the horizontal symmetry. They are suppressed by factor $(\langle F\rangle/\Lambda)^n$, where $\langle F\rangle$ is a breaking scale of H and n is some integer. Thus, the Yukawa hierarchy in $\mathbf{10}$ sector is larger than that in $\overline{\mathbf{5}}$ residing in $\Psi(\mathbf{27},\mathbf{2})$. This explains why the mass hierarchy of the up-quark sector ($Q, U^c \subset \mathbf{10}$) is the largest and the lepton flavor mixing ($L \subset \overline{\mathbf{5}}$) is larger than the quark flavor mixing.

The model predicts the non-universal sfermion masses eq. (2.3) at the leading order. The renormalizable sfermion soft mass terms can be written as

$$V_{\rm soft}^{\rm renorm} = m_0^2\phi(\mathbf{27},\mathbf{2})^{\dagger a}\phi(\mathbf{27},\mathbf{2})_a + m_{30}^2|\phi(\mathbf{27},\mathbf{1})_3|^2, \tag{2.5}$$

where ϕ represents the scalar components of the superfield Ψ. Again, the model has not only a partial (1st-2nd) universality of $\mathbf{10}$-plet sfermions but also a full (1st-3rd) universality of $\overline{\mathbf{5}}$-plet sfermions. The full universality of $\overline{\mathbf{5}}$ sfermions is crucial to satisfy the FCNC and EDM constraints because the unitary matrices that diagonalize the Yukawa matrices for $\overline{\mathbf{5}}$s are expected to have large off-diagonal entries like the MNS (Maki-Nakagawa Sakita) matrix.

In the following, we identify a region of parameter space where both the naturalness and the FCNC constraints are satisfied. In this model, the condition eq. (2.1) can be expressed numerically in terms of the fundamental parameters defined at the cutoff scale as [53]

$$m_Z^2 \simeq -1.9|\mu(\Lambda)|^2 - 1.2m_{H_u}^2(\Lambda) + 1.5m_{30}^2 + 5.9m_{1/2}^2 + \cdots . \tag{2.6}$$

The term proportional to $m_{1/2}$ arises through the stop mass dependence of the RGE. The large cancellation is not required in the right hand side of eq. (2.6) as long as parameters μ, m_{H_u}, m_{30} and $m_{1/2}$ are around the Z boson mass scale. Therefore we study the region of the parameter space where

$$m_{1/2} \lesssim 300\,\text{GeV}, \qquad m_{30},\ m_{H_u}(\Lambda) \lesssim 500\,\text{GeV}. \tag{2.7}$$

In this case, μ is typically 200 to 500 GeV.

The other sfermion masses are given by m_0. If m_0 is also around the Z boson mass scale, FCNCs and EDMs severely constrain the flavor off-diagonal terms of the sfermion mass matrices and CP violating phases of the various SUSY breaking parameters. Such

[1] The numbers in the parenthesis denote representations under $E_6 \times$ SU(2)$_H$

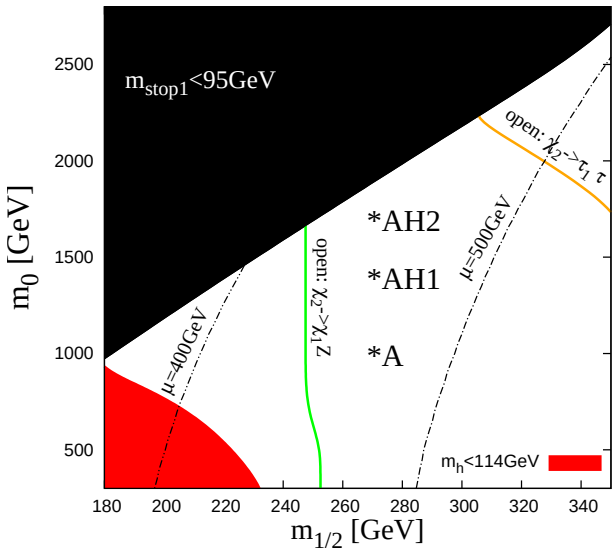

Figure 1. The allowed region on $(m_{1/2} - m_0)$ plane. The other parameters are taken $m_{30} = m_{H_u}(\Lambda) = m_{H_d}(\Lambda) = 300\,\mathrm{GeV}$, $A_0 = -600\,\mathrm{GeV}$, $\tan\beta = 10$, $\mathrm{sgn}(\mu) = +$.

constraints are sometimes problematic to construct explicit models, because various sources that violate the universality are expected.[2] On the other hand, if m_0 is much larger than the weak scale, the constraints can be relaxed.[3]

However, there is upper bound on m_0. A large mass splitting between the first two generations and the 3rd generation sfermions tends to make the 3rd generation sfermion mass squared negative through the 2-loop RG effects, and cause the color and charge breaking (CCB) [55]. In addition, large $\tan\beta$ ($\tan\beta \equiv \langle H_u\rangle/\langle H_d\rangle$) potentially cause the CCB problem in our scenario. The $\mathbf{10}_3$ couple to the $\overline{\mathbf{5}}_3$ through the bottom Yukawa coupling, Y_b. The negative correction to $(m^2_{\tilde{q}})_{33}$ is roughly given as

$$\Delta(m^2_{\tilde{q}})_{33} \sim -\frac{|Y_b|^2}{(4\pi)^2} m^2_{\tilde{b}_R} \ln\left(\frac{\Lambda^2}{m^2_{\tilde{b}_R}}\right). \tag{2.8}$$

Note $m_{\tilde{b}_R} = m_0$ at the cutoff scale. This contribution would be as large as the 2-loop RG effect unless Y_b is sufficiently small. Small $\tan\beta$ ($\tan\beta \sim 10$) is also preferable in E_6 SUSY GUT model with horizontal symmetry. In the models the bottom Yukawa coupling, which is originated from the Yukawa couplings for $\Psi(\mathbf{27}, \mathbf{2})$, is suppressed because it is forbidden under the horizontal symmetry.

In figure 1, we show the allowed region on $(m_{1/2} - m_0)$ plane. Here, the low energy particle spectra are calculated using `ISAJET 7.75` [56]. We fix the other parameters as

[2] The RG effect or the effect of the gravity mediation is one of the sources to produce the non-universality. In models with the horizontal symmetry, the effect of the horizontal symmetry breaking is also the source to produce the non-universality.

[3] The constraint from the up-quark (C)EDM is still severe because some contributions do not decouple with increading m_0. A spontaneous CP violation mechanism may solve this issue [49].

JHEP10(2009)005

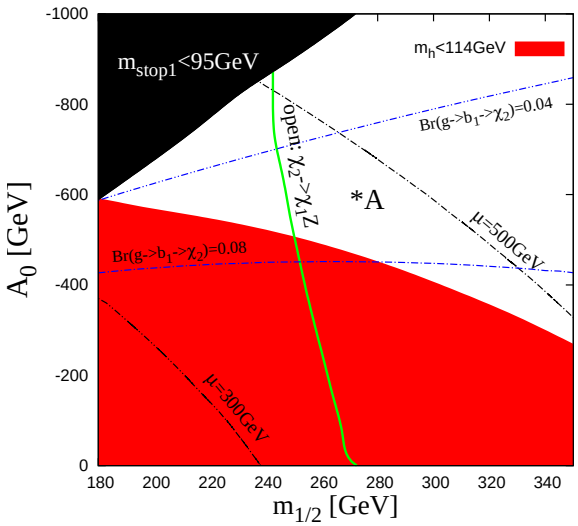

Figure 2. The allowed region on $(m_{1/2} - A_0)$ plane. The other parameters are taken as $m_0 = 1\,\text{TeV}$, $m_{30} = m_{H_u}(\Lambda) = m_{H_d}(\Lambda) = 300\,\text{GeV}$, $\tan\beta = 10$ and $\text{sgn}(\mu) = +$.

$m_{30} = m_{H_u}(\Lambda) = m_{H_d}(\Lambda) = 300\,\text{GeV}$, $A_0 = -600\,\text{GeV}$, $\tan\beta = 10$ and $\text{sgn}(\mu) = +$, where A_0 is the universal trilinear coupling. In the black region the lighter mass eigenstate of stops, $\widetilde{t}_1$, is unacceptably light due to the 1 and 2-loop RG effects. We find that m_0 cannot exceed 2 TeV in the region where $m_{30}, m_{1/2} \lesssim 300\,\text{GeV}$ and $-A_0 \gtrsim 600\,\text{GeV}$. Thus, in this paper we study the parameter region where[4]

$$m_0 \sim 1 - 2\,\text{TeV}, \qquad \tan\beta = 10. \tag{2.9}$$

In the following, we call the scenario characterized by eqs. (2.3), (2.7) and (2.9) *modified universal sfermion mass* (MUSM) *scenario*.

The mass of the lightest CP-even Higgs boson, m_h, tends to be lighter than LEP II SM Higgs mass bound $m_{\varphi_{\text{SM}}} > 114.4\,\text{GeV}$ [57]. To push up m_h above the bound, the quantum correction to the Higgs quartic coupling is crucial [59]. This typically requires large stop masses or a trilinear coupling. Since large m_{30} and $m_{1/2}$ are not preferable in view of the naturalness, we search an allowed region in the direction of large $|A_0|$. Figure 2 shows the allowed region on $(m_{1/2} - A_0)$ plane. The red region is excluded by the condition $m_h > 114\,\text{GeV}$. We find that the Higgs mass bound requires $|A_0| \gtrsim 400 - 600\,\text{GeV}$ in the region where $m_{30}, m_{1/2} \sim 200 - 300\,\text{GeV}$. The two black dashed lines represent $\mu = 300\,\text{GeV}$ and 500 GeV at the stop mass scale. The μ value is not sensitive to A_0 compared with its dependence on $m_{1/2}$ in figure 2. This means the weak scale m_{H_u} is not so sensitive to A_0, and we can take large value of A_0 without making naturalness worse. However a large $|A_0|$ may also cause the CCB problem, because it may lead one of the stop masses squared to be negative. In the black region of figure 2, the lighter stop becomes unacceptably light, $m_{\widetilde{t}_1} < 95\,\text{GeV}$ [58], due to the large $|A_0|$ value.

[4]This scenario however cannot explain the anomaly of the muon $g-2$ [54], because $\widetilde{\mu}$ and $\widetilde{\nu}_\mu$ are heavy due to the large m_0.

JHEP10(2009)005

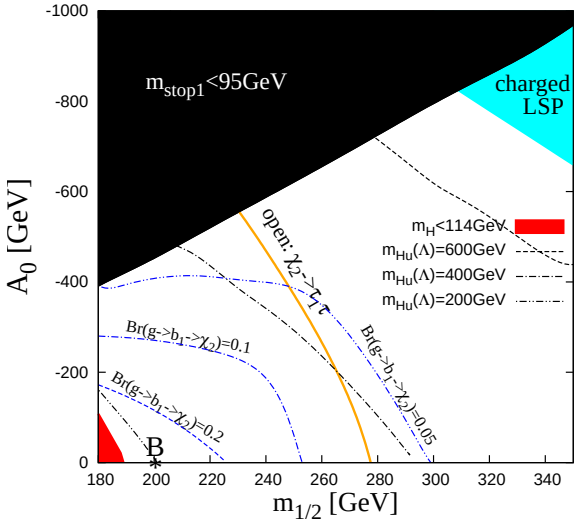

Figure 3. The allowed region on $(m_{1/2}-A_0)$ plane in the light Higgs scenario. The other parameters are taken as $m_0 = 1\,\mathrm{TeV}$, $m_{30} = 200\,\mathrm{GeV}$, $\tan\beta = 10$, $\mu = 250\,\mathrm{GeV}$ and $m_A = 105\,\mathrm{GeV}$.

	Values				
Parameters	A	AH1	AH2	B	U
m_0	1000	1400	1700	1000	1000
m_{30}	300	300	300	200	1000
$m_{1/2}$	270	270	270	200	270
A_0	-600	-600	-600	0	-1600
$\tan\beta$	10	10	10	10	20
$m^2_{H_d}(\Lambda)$	$(300)^2$	$(300)^2$	$(300)^2$	$-(216.0)^2$	$(1000)^2$
$m_{H_u}(\Lambda)$	300	300	300	196.7	1000

Table 1. The parameters of each model point. The unit of mass parameters is GeV .

	Masses (GeV)				
Particles	A	AH1	AH2	B	U
$\widetilde{q}$	1150	1500	1780	1080	1145
$\widetilde{t}_1$	321	262	187	296	281
$\widetilde{b}_1$	540	499	456	400	856
$\widetilde{g}$	697	711	721	537	706
$\widetilde{\chi}^0_1$	110	111	111	77	114

Table 2. The masses of some sparticles at each model point.

To perform Monte Carlo simulation studies we choose a representative parameter set, Point A with $m_0 = 1000\,\mathrm{GeV}$, $m_{30} = 300\,\mathrm{GeV}$ and $m_{1/2} = 270\,\mathrm{GeV}$. The other parameters

JHEP10(2009)005

are listed in table 1. In order to see the m_0 dependence of the collider signature, we also choose model points AH1 and AH2 with $m_0 = 1400$ and 1700 GeV, respectively. These model points are shown in figures 1, 2 and table 1. Point U shown in table 1 is a CMSSM model point which will be investigated in section 4. The masses of some sparticles are shown in table 2.

If Higgs masses can be non-universal, there is another allowed region where the heaviest CP-even Higgs boson, H, becomes the SM-like Higgs boson [60, 61]. This scenario is referred as *a light Higgs scenario* or *an inverted hierarchy scenario*. This can be realized if the CP-odd Higgs boson mass, m_A, satisfies $m_A \sim 100$ GeV, which also prefers small $|\mu|$. Because of the small m_A and μ parameter, the thermal relic density of the $\widetilde{\chi}_1^0$ tends to be the same or small compared with the observed dark matter density [62, 63]. In this scenario all Higgs bosons, h, H, A, $H^{\pm}$, have small masses around the weak scale, therefore they would contribute to various rare B decay processes. Actually, constraints from $Br(B_u^+ \to \tau^+ \nu_\tau)$ [64] and $Br(B_s \to \mu^+ \mu^-)$ [65] exclude $\tan\beta \gtrsim 15$ region [66]. And $Br(b \to s\gamma)$ requires $\mathrm{sign}(\mu) = +$ and small masses of both $\widetilde{t}_i$ and $\widetilde{\chi}_i^{\pm}$ [61], so that the charged Higgs - top quark contribution can cancel with the chargino - stop contribution. The prediction of $Br(b \to s\gamma)$ however depends on the off-diagonal entries of V_{u_R}, V_{u_L} and V_{d_L} in eq. (2.4) [48].

In figure 3, we show the allowed region on $(m_{1/2} - A_0)$ plane. Here we fix $m_0 = 1$ TeV, $m_{30} = 200$ GeV, $\tan\beta = 10$, $\mu = 250$ GeV and $m_A = 105$ GeV. The heavier Higgs boson in the MSSM is the SM like in this case, and LEP II bound should be applied to H. The red region of figure 3 is excluded by the condition $m_H > 114$ GeV. The allowed region is widely extended to the small A_0 region compared with the normal case. We choose Point B defined in table 1 as a representative parameter point.

3 The characteristic signatures of MUSM

3.1 The number of b jets

In MUSM scenario, m_0 is much larger than $m_{1/2}$. Then, the gluino 2-body decay mode into the first two generation squarks, $\widetilde{g} \to \widetilde{q}q$, is closed. On the other hand, in a wide parameter region $\widetilde{t}_1$ and $\widetilde{b}_1$ are lighter than gluino due to the RG running and left-right mixing effects even if $m_{30} \gtrsim m_{1/2}$. Then, $\widetilde{g} \to \widetilde{t}_1 t$ and $\widetilde{b}_1 b$ modes entirely dominate the gluino decay. Since a gluino is a flavor singlet, the gluino decay chain contains at least 2 b jets (b-$\bar{b}$ pairs). Therefore $\widetilde{g}$-$\widetilde{g}$ and $\widetilde{q}$-$\widetilde{g}(\widetilde{q})$ production events have 4 b partons. This characteristic feature can be observed at the LHC by counting the number of b tagged jets.

To simulate the LHC signature at the model points selected in section 2, we calculate the low energy particle spectra and the sparticle decay branching ratios by `ISAJET`. The SUSY events are generated by the parton shower Monte Carlo `HERWIG` [67, 68], and the detector resolutions are simulated by `AcerDET` [69]. We assume the collider center of mass energy is $\sqrt{s} = 14$ TeV. Throughout this paper, we adopt the following SUSY cuts to reduce the SM background:

- $N_{50}^{\mathrm{jets}} \geq 4, \quad N_{100}^{\mathrm{jets}} \geq 1,$

JHEP10(2009)005

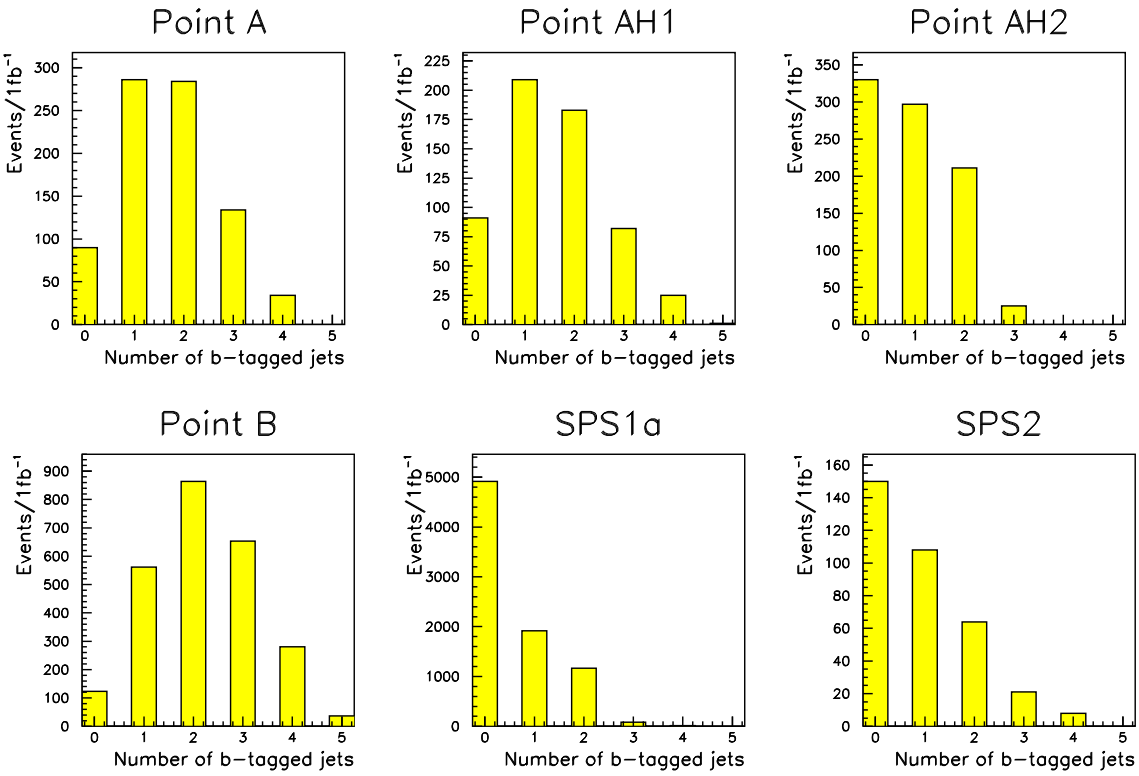

Figure 4. The distribution of the number of b tagged jets per $1\,\mathrm{fb}^{-1}$ at each model point. The b tagging efficiency is assumed to be 60 %.

- $M_{\mathrm{eff}} \equiv \sum_{i=1}^{4} |p_T^{(i)}| + \not{E}_T > 500\,\mathrm{GeV}$,
- $\not{E}_T > \max\{200\,\mathrm{GeV}, 0.2M_{\mathrm{eff}}\}$,

where $p_T^{(i)}$ is the transverse momentum of i-th jet ($p_T^{(i)} > p_T^{(j)}$ for $i < j$) and $N_{50(100)}^{\mathrm{jets}}$ is the number of jets with $p_T > 50(100)\,\mathrm{GeV}$ and $|\eta| < 3$.

The distribution of the number of b jets at each model point is shown in figure 4. Here we count the b tagged jets with $p_T(b) > 50\,\mathrm{GeV}$ and $|\eta(b)| < 2.5$, and require no isolated lepton in the event. The number of SUSY events corresponds to 1 fb^{-1} of the integrated luminosity. We assume the b tagging efficiency is 60 %. To compare the distributions with those of the benchmark model points with universal sfermion masses, the distributions for the SPS1a and SPS2 model points [70] are also shown in figure 4. The peak of the distributions is at zero at SPS1a and SPS2, while zero b tagged events are suppressed at Point A, AH1 and B.

The suppression of no-b jet SUSY events indicates the following mass relation:

$$m_{\tilde{q}} > m_{\tilde{g}} > m_{\tilde{t}_1(\tilde{b}_1)} + m_{t(b)} \qquad \text{or} \qquad m_{\tilde{q}} \gg m_{\tilde{t}_1(\tilde{b}_1)} + m_{t(b)} > m_{\tilde{g}}, \tag{3.1}$$

Indeed in the distributions of mSUGRA benchmark points SPS1a−SPS9, this feature is not seen (See appendix B). Even at SPS2, where ($m_{\tilde{g}}$, $m_{\tilde{q}}$, $m_{\tilde{t}_1}$, $m_{\tilde{b}_1}$) = (796, 1560, 963, 1301) GeV and the gluino branching ratio into $2b + X$ is about 70%, the peak is at zero.

JHEP10(2009)005

Production	Production Ratios (%)				
Processes	A	AH1	AH2	B	U
$\widetilde{g}\widetilde{g}$	32	50	55	47	36
$\widetilde{q}\widetilde{g}$	43	22	9	38	45
$\widetilde{q}\widetilde{q}$	7	2	1	3	9
$\widetilde{t}_1\widetilde{t}_1$	9	14	19	5	5
$\widetilde{b}_1\widetilde{b}_1$	2	5	9	3	0
others	7	6	7	4	5
Total Events	1484	984	1096	3468	1677

Table 3. The number of SUSY events after standard SUSY cut at $\int \mathcal{L}dt = 1$ fb^{-1}. Here we use the same character for a particle and the antiparticles.

An exceptional case is Point AH2. At this point, the distribution peaks at zero, although the mass relation eq. (3.1) is satisfied. At this point the $\widetilde{t}_1$ is as light as top quark, $m_{\widetilde{t}_1} = 187\,\text{GeV}$, due to the large m_0 value ($m_0 = 1700\,\text{GeV}$), and the 2-body decay modes $\widetilde{t}_1 \to \chi_1^+ b$ and $\widetilde{t}_1 \to \widetilde{\chi}_1^0 t$ are closed. Then the flavor violating 2-body decay mode $\widetilde{t}_1 \to \widetilde{\chi}_1^0 c$ dominates the $\widetilde{t}_1$ decay [71]. In such case, the distribution of the number of b jets are not helpful for the model discriminations. It has been shown in [72] that such a light stop may be detected at the LHC in $\gamma + \not{E}_T$ or $j + \not{E}_T$ channel.

3.2 The highest p_T jet

In MUSM scenario, there is large mass splitting between m_0 and $m_{1/2}$, m_{30}, but m_0 is bounded above by the CCB constraint. The 1st and 2nd generation squarks, $\widetilde{q}$, may be produced enough to be seen at the LHC. The number of SUSY events after the standard SUSY cuts at $\int \mathcal{L}dt = 1\,\text{fb}^{-1}$ are listed in table 3.

The SUSY production is dominated by $\widetilde{g}$-$\widetilde{g}$ and $\widetilde{q}$-$\widetilde{g}$ production processes at Points A, AH1 and B. On the other hand, the fraction of $\widetilde{q}$-$\widetilde{g}(\widetilde{q})$ production is relatively small (10 %) at Point AH2, due to the very large m_0 value ($m_0 = 1700\,\text{GeV}$). The fractions of $\widetilde{t}$-$\widetilde{t}$ and $\widetilde{b}$-$\widetilde{b}$ productions are also small at all model points. These events hardly survive the standard SUSY cut due to the small masses of $\widetilde{t}_1$ and $\widetilde{b}_1$.

Once a heavy squark is produced, it decays mainly into $\widetilde{g}+q$. The quark jet is expected to have relatively large transverse momentum since the mass difference between $\widetilde{g}$ and $\widetilde{q}$ is large. The order of the transverse momentum is around $m_{\widetilde{q}}/2$. This quark jet tends to be the highest p_T jet in the event.

We show the p_T distribution of the highest p_T jet at each model point in figure 5. Here we require that the rapidity of the highest p_T jet is less than 1.5 ($|\eta(j^{1\text{st}})| < 1.5$) and the jet is not b tagged. The number of the generated events corresponds to $\int \mathcal{L}dt = 1$ fb^{-1}. In the figures the yellow histograms represent the contribution of $\widetilde{g}$-$\widetilde{g}$ and $\widetilde{t}$-$\widetilde{t}$ productions, while the shaded histograms represent that of $\widetilde{g}$-$\widetilde{q}$ and $\widetilde{q}$-$\widetilde{q}$ productions. The p_T distribution of squark productions tends to be harder than that of gluino pair production. This is

JHEP10(2009)005

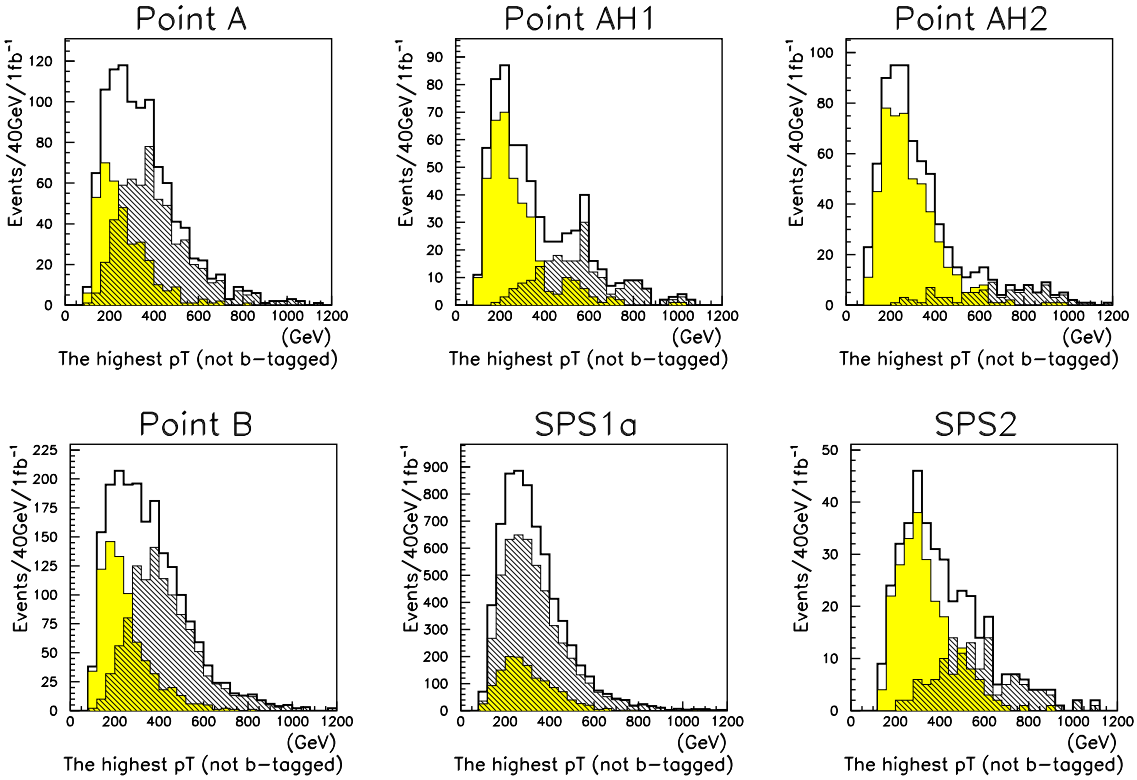

Figure 5. The p_T distribution of the non-b tagged highest p_T jet in the event at each model points.

the contribution of the hard jet from the heavy squark decay. Indeed, as m_0 increases ($m_0 = 1400$, 1700 GeV at Points AH1 and AH2), the peak of the shaded distribution moves to the high energy side. At the same time, the number of the events coming from squark production decreases significantly.

The difference between the yellow and shaded distribution indicates

$$m_{\tilde{q}} - m_{\tilde{g}} \gg \max\{m_{\tilde{g}} - m_{\tilde{t}_1(\tilde{b}_1)} - m_{t(b)},\, m_{\tilde{t}_1(\tilde{b}_1)} - m_{\tilde{\chi}_1^0}\}\,, \tag{3.2}$$

under the mass relation eq. (3.1).

In order to see the contributions from gluino pair production separately, we can use the distribution of the b tagged jets. If the highest jet is a b jet, the jet is not originated from the first two generation squark decay. The contribution from the heavy squark decay can be removed by requiring that the highest p_T jet is a b jet. In figure 6, we show the p_T distribution of the b tagged highest p_T jet. The heavy squark contributions (the shaded histograms) are significantly suppressed in the figures. The difference between the distributions of non-b tagged jets and b tagged jets suggests the large mass splitting between $\tilde{g}$ and $\tilde{q}$.

For comparison, we have done the same analysis for the benchmark model points SPS1a−SPS9 (See appendix B). There is no clear difference between the "b tagged" and "non-b tagged" distributions except at SPS2. At SPS2 the universal scalar mass, $m_0 =$ 1450 GeV, is much larger than the universal gaugino mass, $m_{1/2} = 300$ GeV. So the decay

JHEP10(2009)005

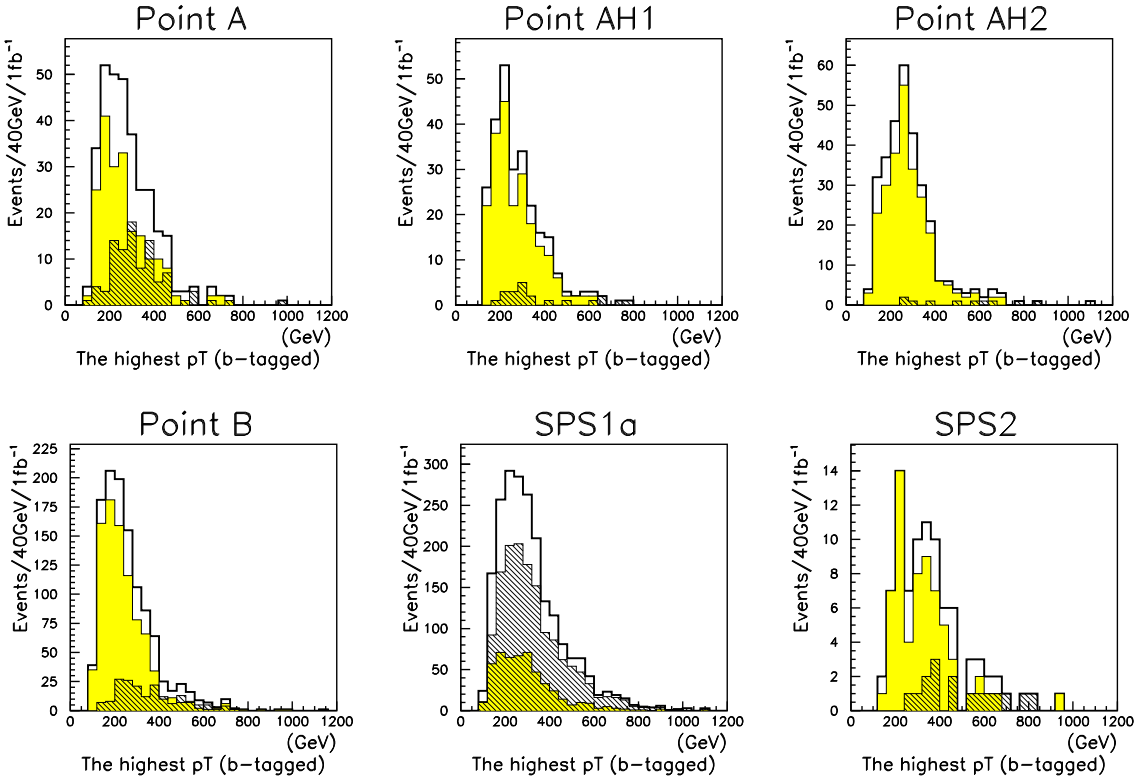

Figure 6. The p_T distribution of the b tagged highest p_T jet in the event at each model points.

of the 1st generation squarks produce the hard jet, while the gluino 3-body decays cannot produce hard b jets.

4 "Look alike" in CMSSM

The characteristic signatures of MUSM scenario in the number of b tagged jets and the $p_T^{(1)}$ distributions do not eliminate the possibility of the universal (CMSSM type) boundary condition of soft masses at the cutoff scale, though they are good indication of MUSM scenario. In this section we study a region of parameter space in CMSSM whose signature is similar to that of MUSM scenario, and seek for the outstanding observable that is useful to distinguish MUSM scenario from the CMSSM parameter region.

If one takes $m_0 \gg m_{1/2}$ in CMSSM, the $p_T^{(1)}$ distributions of b tagged and non-b tagged jets is similar to that of MUSM scenario as we have seen at SPS2. When one fixes m_0 and $m_{1/2}$, CMSSM still has the other 2 free parameters A_0 and $\tan\beta$. We scan $(\tan\beta - A_0)$ parameter space with fixing $m_0 = 1\,\mathrm{TeV}$, $m_{1/2} = 270\,\mathrm{GeV}$ and $\mathrm{sign}(\mu) = +$ in figure 7. In a gray region, $\widetilde{g} \to \widetilde{t}_1 t$ mode is open and it entirely dominates the gluino decay. Therefore there will be 4 b partons in the final state as in MUSM scenario. We choose such a model point U as a representative parameter point. The parameters are listed in table 1 and the sparticle masses are listed in table 2.

JHEP10(2009)005

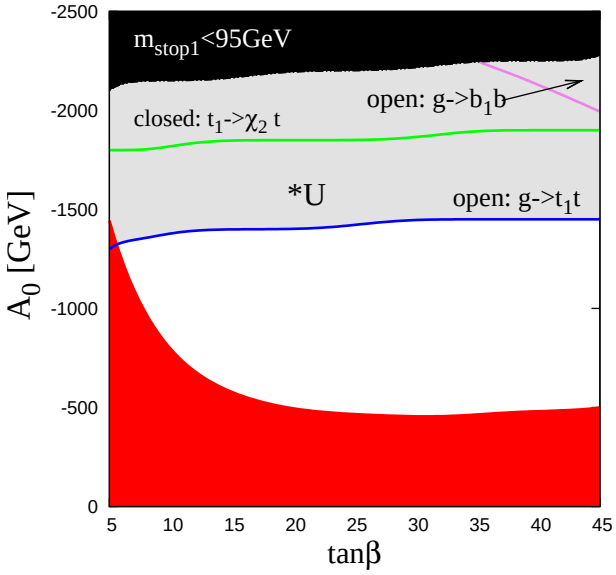

Figure 7. The thresholds of the 2-body decays on the $(\tan\beta - A_0)$ parameter plane. Other parameters are chosen as $m_0 = m_{H_u}(\Lambda) = m_{H_d}(\Lambda) = 1000\,\mathrm{GeV}$, $m_{1/2} = 270\,\mathrm{GeV}$, $\mathrm{sgn}(\mu) = +$.

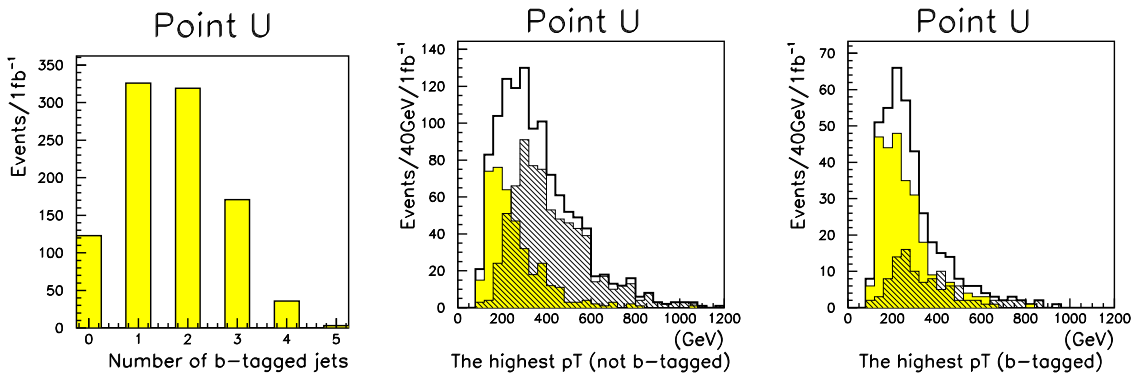

Figure 8. The distributions of the number of b jets (Left) and the p_T of the highest p_T jet for non-b tagged(Center) and b tagged(Right) jets at point U.

We show the number of b tagged jets and the $p_T^{(1)}$ distributions at Point U in figure 8. The distributions are similar to those of MUSM scenario. This means the analysis presented in the previous section cannot discriminate MUSM scenario from the gray region in CMSSM, though the soft masses are universal at the cutoff scale. Therefore more information is required to distinguish these two scenarios.

There are some differences in gluino decay branching ratios. In CMSSM case, the gluino decay can be dominated only by $\widetilde{g} \to \widetilde{t}_1 t$ mode. If one takes a large $\tan\beta$ along with a large $|A_0|$, $\widetilde{g} \to \widetilde{b}_1 b$ mode is open as shown in figure 7. However $\widetilde{t}_1$ is much lighter than $\widetilde{b}_1$ in this region, and $Br(\widetilde{g} \to \widetilde{b}_1 b)$ cannot be significant. On the other hand, $Br(\widetilde{g} \to \widetilde{b}_1 b)$ can be as large as $Br(\widetilde{g} \to \widetilde{t}_1 t)$ in MUSM scenario, unless $\widetilde{t}_1$ is extremely lighter than $\widetilde{b}_1$

JHEP10(2009)005

due to the large $|A_0|$ effect. Therefore we can regard a sizable $Br(\widetilde{g} \to \widetilde{b}_1 b)$ as an indication of MUSM scenario.

Distinction of $\widetilde{g} \to \widetilde{b}_1 b$ decay from $\widetilde{g} \to \widetilde{t}_1 t$ decay is not so easy at these model points. A difficulty comes from similarity of final states of these two decay modes. The main decay chains of $\widetilde{t}_1$ and $\widetilde{b}_1$ are as follows.

$$\begin{aligned}
&\widetilde{t}_1 \to \chi_1^\pm b \to \widetilde{\chi}_1^0 W^{(*)} b \quad \cdots (a) \qquad \widetilde{b}_1 \to \widetilde{t}_1 W^{(*)} \quad \cdots (d) \\
&\quad \to \widetilde{\chi}_1^0 t \quad \cdots (b) \qquad \quad \to \chi_1^\pm t \to \widetilde{\chi}_1^0 W^{(*)} t \quad \cdots (e) \\
&\quad \to \widetilde{\chi}_2^0 t \to \widetilde{\chi}_1^0 Z^{(*)} t \quad \cdots (c) \qquad \quad \to \widetilde{\chi}_2^0 b \to \widetilde{\chi}_1^0 Z^{(*)} b \quad \cdots (f)
\end{aligned} \tag{4.1}$$

Here we ignore $\widetilde{b}_1 \to \widetilde{\chi}_1^0 b$ mode because the branching ratio is tiny due to the hypercharge and $\mathrm{U}(1)_Y$ gauge coupling suppression if $\widetilde{b}_1 \sim \widetilde{b}_L$ and the $\widetilde{\chi}_1^0$ is bino-like. In MUSM scenario or in the gray region of CMSSM, $\widetilde{\chi}_1^\pm \to \widetilde{l}\nu(\widetilde{\nu}l)$ and $\widetilde{\chi}_2^0 \to \widetilde{l}\widetilde{l}(\widetilde{\nu}\nu)$ modes are not open due to a large m_0. Therefore we assume $\chi_1^\pm \to \widetilde{\chi}_1^0 W$ and $\widetilde{\chi}_2^0 \to \widetilde{\chi}_1^0 Z$ modes are open and dominate $\chi_1^\pm$ and $\widetilde{\chi}_2^0$ decay. Except for the decay modes (c) and (f), $\widetilde{g} \to \widetilde{t}t$ and $\widetilde{g} \to \widetilde{b}_1 b$ have the same final state $2W + 2b + \widetilde{\chi}_1^0$.

The decay modes (c) and (f) are useful although their branching ratios are less than 10% in a wide parameter region. The final states of the gluino decay via the decay modes (c) and (f) are $2W + 2b + Z + \widetilde{\chi}_1^0$ and $2b + Z + \widetilde{\chi}_1^0$, respectively. If one of the W bosons decays into jets, the number of associate jets is differ by 2 between these modes.

We show the distributions of the number of the jets with $p_T > 50\,\mathrm{GeV}$ and $|\eta| < 2.5$, (N^{jets}) in events with a $Z \to l_i^+ l_i^-$ candidate at Point A and U in figure 9. We require there are opposite sign same flavor (OSSF) lepton pairs with $p_T > 15\,\mathrm{GeV}$ and $|\eta| < 3$ whose invariant mass satisfy $|m_{ll} - m_Z| < 5\,\mathrm{GeV}$.[5] To reduce an additional Z boson source from $\widetilde{q} \to \widetilde{\chi}_2^0 q \to \widetilde{\chi}_1^0 Z q$, we adopt $\widetilde{g}$-$\widetilde{g}$ selection cuts:

- The highest p_T jet is b tagged,
- $p_T^{(1)} < 300\,\mathrm{GeV}$.

The shaded histograms in these figures represent the contribution from the $\widetilde{q}$-$\widetilde{g}$ and $\widetilde{q}$-$\widetilde{q}$ production events. The contamination from the squark decay $\widetilde{q} \to \widetilde{\chi}_2^0 q \to \widetilde{\chi}_1^0 Z q$ is negligible after the $\widetilde{g}$-$\widetilde{g}$ selection cuts.

At Point A the peak is at $N^{\mathrm{jets}} = 4$, while the peak is at $N^{\mathrm{jets}} = 6$ at Point U. This suggests that the Z boson comes from $\widetilde{b}_1$ decay at Point A, while it comes from $\widetilde{t}_1$ decay at Point U. By this analysis, we can discriminate MUSM scenario from the CMSSM parameter region, though a large integrated luminosity may be required.[6]

[5] If $\widetilde{\chi}_2^0 \to \widetilde{\chi}_1^0 Z$ mode is not open, the distribution of two lepton invariant mass would show kinematical edge induced by $\widetilde{\chi}_2^0 \to \widetilde{\chi}_1^0 l_i^+ l_i^-$ mode as shown in section 5.1.2. In this case, we should require $m_{ll}^{\mathrm{edge}} - m_{ll} < 10\,\mathrm{GeV}$ instead of $|m_{ll} - m_Z| < 5\,\mathrm{GeV}$.

[6] Note in the region above a green line in figure 7, the decay mode (c) in eq. (4.1) is closed. In this region, Z boson does not come from $\widetilde{g}$ decay in CMSSM, so the discrimination from this region is easy.

JHEP10(2009)005

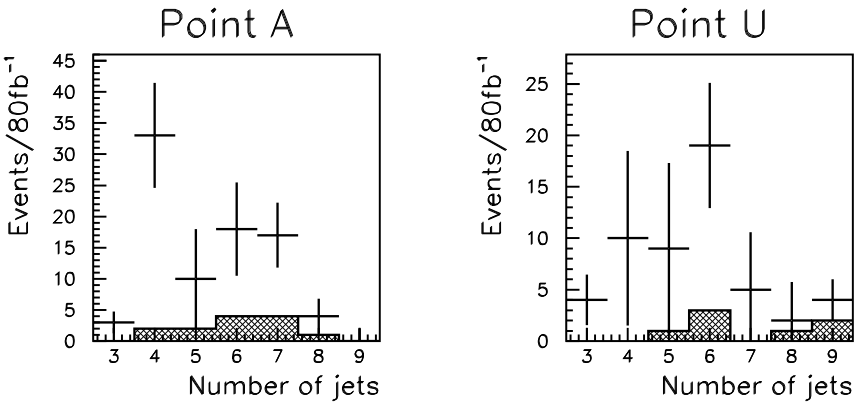

Figure 9. The distributions of the number of jets in the event with $Z \to l_i^+ l_i^-$ at Point A and U.

5 The sparticle mass measurement

5.1 Exclusive analyses

5.1.1 Conditions to have OSSF lepton pair signature in MUSM scenario

SUSY particle masses may be determined by measuring the kinematical endpoints of sparticle decay products. Especially, the distribution of the events with OSSF leptons coming from $\widetilde{\chi}_2^0 \to \widetilde{l}_i^{\pm} l_i^{\mp} \to \widetilde{\chi}_1^0 l_i^{\pm} l_i^{\mp}$ are useful [4–7, 18, 19]. However, there are several reasons for this channel may not be available in MUSM scenario.

In this scenario gluino entirely decays into the 3rd generation squarks, $\widetilde{t}_1$ and $\widetilde{b}_1$. From a phase space consideration $Br(\widetilde{t}_1 \to \widetilde{\chi}_1^+ b) \gg 2Br(\widetilde{t}_1 \to \widetilde{\chi}_2^0 t)$ and $Br(\widetilde{t}_1 \to \widetilde{\chi}_1^0 t) \gg Br(\widetilde{t}_1 \to \widetilde{\chi}_2^0 t)$, where the factor 2 in the first relation comes from the Dirac nature of the chargino. Thus, $\widetilde{t}_1 \to \widetilde{\chi}_1^+ b$ and $\widetilde{t}_1 \to \widetilde{\chi}_1^0 t$ dominate the stop decay. If the gluino decay is dominated by $\widetilde{g} \to \widetilde{t}_1 t$ mode, $\widetilde{\chi}_2^0$ does not appear with sufficiently high rate in the gluino cascade decays.

In this scenario the $\widetilde{b}_1$ branching ratio into $\widetilde{\chi}_2^0$ may also be small, though gluino can decay into $\widetilde{b}_1 b$. Assuming $Y_b = 0$, $\widetilde{\chi}_2^0 = \widetilde{W}_3$ and $\widetilde{b}_1 = \widetilde{b}_L$, the tree level formulae of the $\widetilde{b}_1 \to \widetilde{\chi}_2^0 b$ and $\widetilde{b}_1 \to \widetilde{t}_1 W$ decay widths are given by [73]

$$\Gamma(\widetilde{b}_1 \to \widetilde{\chi}_2^0 b) \simeq \frac{g^2 m_{\widetilde{b}_1}}{32\pi}\left(1 - \frac{m_{\widetilde{\chi}_2^0}^2}{m_{\widetilde{b}_1}^2}\right)^2, \tag{5.1}$$

$$\Gamma(\widetilde{b}_1 \to \widetilde{t}_1 W) \simeq \frac{g^2 m_{\widetilde{b}_1}}{32\pi}\overline{\lambda}^{3/2}(x_{\widetilde{t}_1}, x_W)\left(\frac{a_t^2 m_{\widetilde{b}_1}^2}{(m_{\widetilde{t}_L}^2 - m_{\widetilde{t}_1}^2)^2 + a_t^2 m_t^2}\right)\left(\frac{m_t^2}{m_W^2}\right), \tag{5.2}$$

where $x_{\widetilde{t}_1} = m_{\widetilde{t}_1}^2/m_{\widetilde{b}_1}^2$, $x_W = m_W^2/m_{\widetilde{b}_1}^2$ and $\overline{\lambda}(x,y) = 1 + x^2 + y^2 - 2(x + y + xy)$ and $a_t = (A_t - \mu \cot\beta)$. In eq. (5.2) $\Gamma(\widetilde{b}_1 \to \widetilde{t}_1 W)$ has a enhancement factor (m_t^2/m_W^2). Thus, $\widetilde{b}_1$ decays dominantly into $\widetilde{t}_1 W$ unless it is kinematically suppressed.

In MUSM scenario, the first two generation sfermions are much heavier than the second lightest neutralino. Therefore the 2-body decay mode of $\widetilde{\chi}_2^0$ into the first two generation sleptons $\widetilde{\chi}_2^0 \to \widetilde{l}_i^{\pm} l_i^{\mp}$ is kinematically forbidden. The OSSF leptons may arise from the

JHEP10(2009)005

3-body decay mode $\widetilde{\chi}_2^0 \to \widetilde{\chi}_1^0 l_i^{\pm} l_i^{\mp}$ from the off-shell Z boson exchange. If the 2-body decay mode $\widetilde{\chi}_2^0 \to \widetilde{\chi}_1^0 Z$ is open, it dominates the $\widetilde{\chi}_2^0$ decay.

In summary, the sparticle mass measurement using the exclusive analysis with OSSF leptons may work if following conditions are satisfied:

(i)	$\widetilde{g} \to \widetilde{t}_1 t$ mode does not dominate the gluino decay.	
(ii)	$\widetilde{b}_1 \to \widetilde{t}_1 W$ mode is kinematically suppressed.	(5.3)
(iii)	$\widetilde{\chi}_2^0 \to \widetilde{\chi}_1^0 Z$ mode is kinematically forbidden.	

The three conditions can be satisfied when the mass differences $m_{\widetilde{b}_1} - m_{\widetilde{t}_1}$ and $m_{\widetilde{\chi}_2^0} - m_{\widetilde{\chi}_1^0}$ are small, and it can be realized for small $m_{1/2}$ and $|A_0|$. If all conditions are satisfied, a gluino cascade chain,

$$\widetilde{g} \to \widetilde{b}_1 b^{(1)} \to \widetilde{\chi}_2^0 b^{(1)} b^{(2)} \to \widetilde{\chi}_1^0 b^{(1)} b^{(2)} l_i^+ l_i^-, \tag{5.4}$$

can have enough branching fraction. Here subscripts of the b quarks in eq. (5.4) are used to distinguish two b quarks appear subsequently.

The low energy mass spectra and the decay branching ratios of various sparticles at Points A and B are shown in table 4 in appendix A. At Point A, the three conditions in eq. (5.3) are not satisfied. On the other hand, at point B all of the three conditions are satisfied due to the very low SUSY breaking scales, $m_{1/2} = m_{30} = 200\,\mathrm{GeV}$ and $A_0 = 0\,\mathrm{GeV}$.

5.1.2 The exclusive analysis using $\widetilde{\chi}_2^0 \to \widetilde{\chi}_1^0 l_i^+ l_i^-$ channel at Point B

At Point B, SUSY events contain the cascade decay chain (5.4). The OSSF lepton pair from the decay chain is relatively clean signal [4–7, 18, 19]. The background distributions of fake OSSF leptons can be estimated by distributions of OSOF leptons. The kinematical maximum of the two lepton invariant mass coming from $\widetilde{\chi}_2^0 \to \widetilde{\chi}_1^0 l_i^+ l_i^-$ at Point B is given by

$$m_{l_i^+ l_i^-}^{\max} = m_{\widetilde{\chi}_2^0} - m_{\widetilde{\chi}_1^0} = 61\,\mathrm{GeV}. \tag{5.5}$$

The distribution is shown in figure 10. Throughout this section, leptons are required to satisfy $p_T > 15\,\mathrm{GeV}$ and $|\eta| < 3$.

For the decay chain (5.4), the invariant mass distributions m_{bb}, $m_{l_i^+ l_i^- b^{(1)}}$, $m_{l_i^+ l_i^- b^{(2)}}$ and $m_{bb l_i^+ l_i^-}$ may determine sparticle masses. Their kinematical maxima at Point B are given as

$$m_{bb}^{\max} = m_{\widetilde{g}} \sqrt{\left(1 - \frac{m_{\widetilde{b}_1}^2}{m_{\widetilde{g}}^2}\right)\left(1 - \frac{m_{\widetilde{\chi}_2^0}^2}{m_{\widetilde{b}_1}^2}\right)} = 336\,\mathrm{GeV}, \tag{5.6}$$

$$m_{l_i^+ l_i^- b^{(1)}}^{\max} = m_{\widetilde{g}} \sqrt{\left(1 - \frac{m_{\widetilde{b}_1}^2}{m_{\widetilde{g}}^2}\right)\left(1 - \frac{m_{\widetilde{\chi}_1^0}^2}{m_{\widetilde{\chi}_2^0}^2}\right)} = 296\,\mathrm{GeV}, \tag{5.7}$$

$$m_{l_i^+ l_i^- b^{(2)}}^{\max} = m_{\widetilde{b}_1} - m_{\widetilde{\chi}_1^0} = 322\,\mathrm{GeV}, \tag{5.8}$$

$$m_{l_i^+ l_i^- bb}^{\max} = m_{\widetilde{g}} - m_{\widetilde{\chi}_1^0} = 460\,\mathrm{GeV}. \tag{5.9}$$

Since there are typically 4 b partons in the SUSY events, the invariant mass distributions suffer from the combinatorial background. To reduce the background, we adopt

JHEP10(2009)005

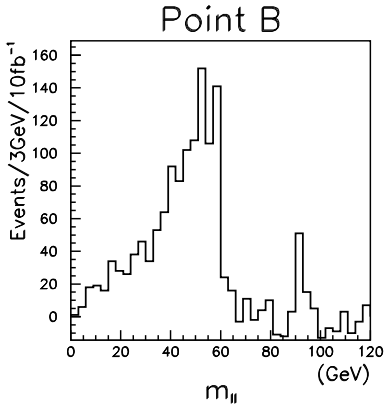

Figure 10. The invariant mass distributions of $l_i^+ l_i^-$. The background distributions estimated from OSOF leptons are subtracted. The number of events corresponds to $\int \mathcal{L}dt$ =10 fb^{-1}.

hemisphere method [76, 77]. The method divides jets and leptons from cascade decay chains into two groups called hemispheres whose entries are much likely to originate from the same mother particle. The groups are defined by hemisphere momenta,

$$p_{\rm hemi}^{(1)} = \sum_i p_i^{(1)}, \quad p_{\rm hemi}^{(2)} = \sum_i p_i^{(2)}, \tag{5.10}$$

where $p_i^{(1)}$ and $p_i^{(2)}$ are jet or lepton momenta that satisfy

$$d(p_{\rm hemi}^{(1)}, p_i^{(1)}) < d(p_{\rm hemi}^{(2)}, p_i^{(1)}), \qquad d(p_{\rm hemi}^{(2)}, p_i^{(2)}) < d(p_{\rm hemi}^{(1)}, p_i^{(2)}). \tag{5.11}$$

Here the function d is defined by

$$d(p_{\rm hemi}^{(i)}, p_k) = (E_{\rm hemi}^{(i)} - |p_{\rm hemi}^{(i)}| \cos\theta_{ik}) \frac{E_{\rm hemi}^{(i)}}{(E_{\rm hemi}^{(i)} + E_k)^2}, \tag{5.12}$$

where θ_{ik} is an angle between $p_{\rm hemi}^{(i)}$ and p_k. We require that jets involved in hemisphere satisfy $p_T > 50\,\text{GeV}$ and $|\eta| < 2.5$ to reduce the contamination of soft jets. To find the two groups of jets and leptons that satisfy eq. (5.10), we first choose the highest p_T jet and the jet with the largest $p_T \Delta R$ as p_1(seed) and p_2(seed), where $\Delta R = \sqrt{\Delta\phi^2 + \Delta\eta^2}$ is the angle difference between the jet and the highest jet. Next we group jets into two groups under the condition $d(p^{(1)}(\text{seed}), p_i^{(1)}) < d(p^{(2)}(\text{seed}), p_i^{(1)})$ etc.. Then axis momenta are defined as $p^{(1)}(\text{ax}) = \sum p_i^{(1)}$, $p^{(2)}(\text{ax}) = \sum p_i^{(2)}$. For the axis momenta, new groups are defined so that $d(p^{(1)}(\text{ax}), p_i^{(1)}) < d(p^{(2)}(\text{ax}), p_i^{(1)})$ etc.. The procedure is iterated several times so that assignment converges.

Although the probability that hemisphere correctly reconstructs original cascade chains is not so high, this method has an advantage for endpoint analyses. In the algorithm, two objects whose momentum directions are roughly the same each other tend to be in the same hemisphere due to eqs. (5.11) and (5.12). Because of this property, any invariant mass distribution of jets and leptons in the same hemisphere tends to be lower than that in the

JHEP10(2009)005

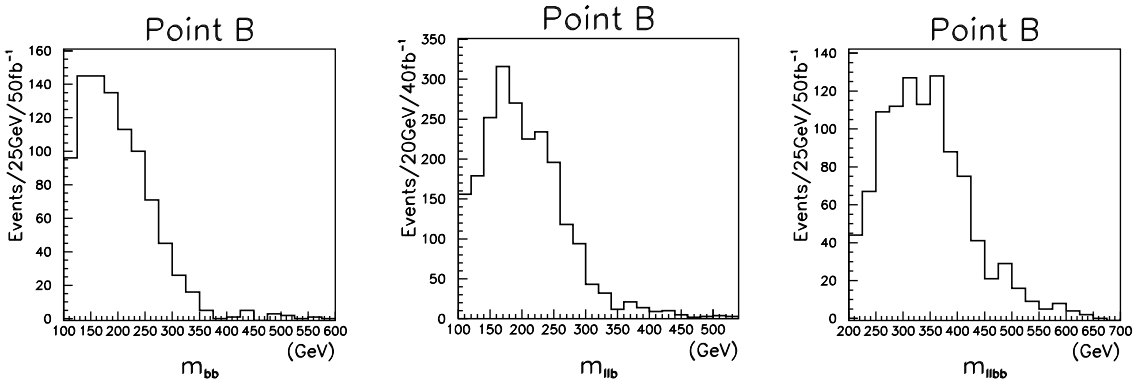

Figure 11. The invariant mass distributions of bb (Left), $bl_i^+l_i^-$ (Center) and $l_i^+l_i^-bb$ (Right). The background distributions estimated from OSOF leptons are subtracted. The corresponding luminosities are $\int \mathcal{L}dt$ =50, 40 and 50 fb^{-1} for the left, center and right distributions.

different hemispheres. Therefore wrong combinations whose invariant mass exceed the signal endpoint are removed with high probability if we take jet pairs in the same hemisphere.

We show the invariant mass distributions of bb, $l_i^+l_i^-b$ and $l_i^+l_i^-bb$ in figure 11. Here all b jets and leptons are required to be in the same hemisphere. If there are more than one or two b jet candidates, we take high p_T b jets. We also require $m_{l_i^+l_i^-} \leq m_{l_i^+l_i^-}^{\max}$ to reduce background OSSF leptons from Z boson decay. The distributions have endpoints near the theoretical expected values shown in eq. (5.6) to (5.9). However bb distribution does not show expected sharp edge structure due to the hemisphere selection.

At this stage, we have 4 measured values $m_{l_i^+l_i^-}^{\max}$, $m_{bb}^{\max}$, $m_{l_i^+l_i^-b}^{\max}$ and $m_{l_i^+l_i^-bb}^{\max}$ for 4 unknown sparticle masses $m_{\widetilde{\chi}_1^0}$, $m_{\widetilde{\chi}_2^0}$, $m_{\widetilde{b}_1}$ and $m_{\widetilde{g}}$. By solving 4 equations, (5.5), (5.6), (5.8) and (5.9), we can get all sparticle masses appeared in the decay chain (5.4) in the stage around 50 fb^{-1} at Point B.

In addition, we can check our results by selecting the events near m_{ll} endpoint. The two lepton system from the 3-body decay $\widetilde{\chi}_2^0 \to \widetilde{\chi}_1^0 l_i^+ l_i^-$ must be at rest in the $\widetilde{\chi}_2^0$ rest frame when $m_{l_i^+l_i^-} = m_{l_i^+l_i^-}^{\max}$. The $\widetilde{\chi}_2^0$ momentum can be estimated from a velocity of the two lepton system for the events with $m_{l_i^+l_i^-} \lesssim m_{l_i^+l_i^-}^{\max}$, if $m_{\widetilde{\chi}_2^0}$ is known [4, 19]. Using the observed $\widetilde{\chi}_2^0$ mass from 4 endpoint measurements, (5.5), (5.6), (5.8) and (5.9), we can calculate the invariant mass distribution of $\widetilde{\chi}_2^0 + b$ from estimated $\widetilde{\chi}_2^0$ momentum. For the decay chain (5.4), the peak of the $m_{\widetilde{\chi}_2^0 b^{(2)}}$ distribution gives the $\widetilde{b}_1$ mass. We show the $m_{\widetilde{\chi}_2^0 b}$ distribution in figure 12 (Left). Here we use events that satisfy $0\,\mathrm{GeV} \leq m_{l_i^+l_i^-}^{\max} - m_{l_i^+l_i^-} \leq 10\,\mathrm{GeV}$. Here we use all b tagged jets and leptons as the candidates because only a few events survive under the requirement that all b jets and leptons are in the same hemisphere. The distribution has a peak near the correct $\widetilde{b}_1$ mass, $m_{\widetilde{b}_1} = 400\,\mathrm{GeV}$.

By using events around the $\widetilde{b}_1$ peak, we can subsequently estimate the $\widetilde{b}_1$ momentum, and calculate the invariant mass of $\widetilde{b}_1 b$. For the decay chain (5.4), the $\widetilde{g}$ mass can be measured from the peak of the $m_{\widetilde{b}_1 b^{(1)}}$ distribution. We show the $m_{\widetilde{b}_1 b}$ distribution in the

JHEP10(2009)005

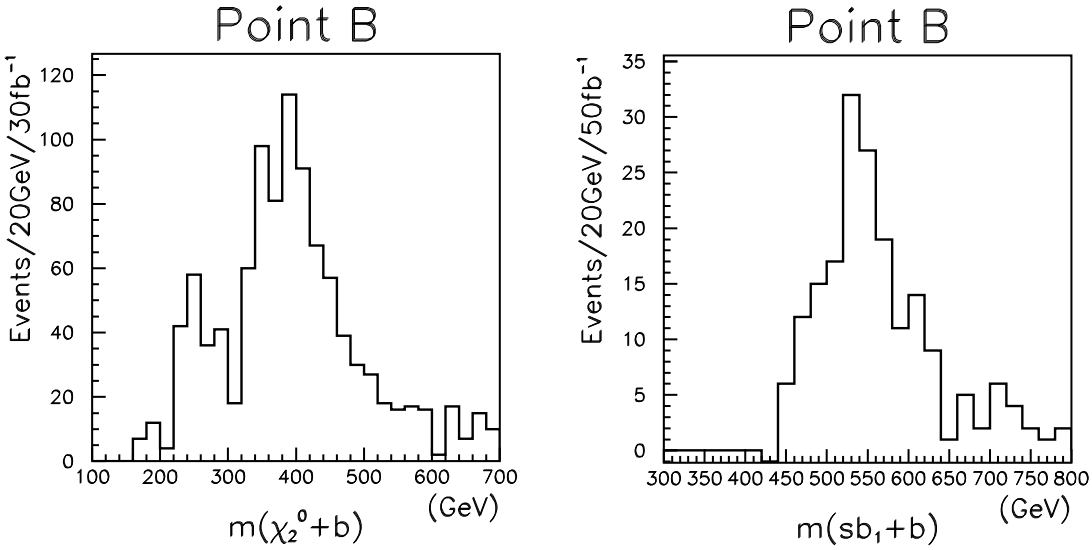

Figure 12. The invariant mass distributions of $\widetilde{\chi}_2^0 b$ (Left) and $\widetilde{b}_1 b$ (Right). In the left figure 4 momenta of the $\widetilde{\chi}_2^0$ are estimated from the velocity of the lepton pair system whose invariant mass satisfies $0\,\text{GeV} \leq m_{l_i^+ l_i^-}^{\max} - m_{l_i^+ l_i^-} \leq 10\,\text{GeV}$ by assuming correct $\widetilde{\chi}_2^0$ mass. In the right figure, momentum of $\widetilde{\chi}_2^0 b$ system whose invariant mass satisfies $|m_{\widetilde{\chi}_2^0 b}^{\text{peak}} - m_{\widetilde{\chi}_2^0 b}| \leq 15\,\text{GeV}$ is regarded as $\widetilde{b}_1$ momentum. The corresponding luminosities are $\int \mathcal{L}dt$ =30 fb^{-1} (Left) and 50 fb^{-1} (Right).

right figure in figure 12. Here we use events that satisfy $|m_{\widetilde{\chi}_2^0 b}^{\text{peak}} - m_{\widetilde{\chi}_2^0 b}| \leq 15\,\text{GeV}$. The distribution has a peak near the correct $\widetilde{g}$ mass, $m_{\widetilde{g}} = 537\,\text{GeV}$.

5.1.3 Top reconstruction and the tb endpoint at Point A

The sparticle mass measurement is challenging for the class of the points A, AH1, AH2. The gluino entirely decays into $\widetilde{t}_1$ and $\widetilde{b}_1$, and decay modes of the $\widetilde{t}_1$ and $\widetilde{b}_1$ are dominated by (a), (b) and (d), (e) in eq. (4.1), respectively. All these cascade chains have the same decay products $2b + 2W + \widetilde{\chi}_1^0$, and a gluino pair system leads to $4b + 4W + \not{E}_T$.[7] Therefore, any exclusive analysis using jets suffers from a large combinatorial background. The gluino decay products contain a top quark with high probability. If the top quark is detected with a significant rate in SUSY events, it indicates the existence of the light 3rd generation squarks.

The lighter stop mass is relatively light at Point A, $m_{\widetilde{t}_1} = 321\,\text{GeV}$, and the phase space of the decay is not small, $m_{\widetilde{g}} - (m_{\widetilde{t}_1} + m_t) \simeq 200\,\text{GeV}$. The top quark from the gluino decay, $\widetilde{g} \to \widetilde{t}_1 t$, is boosted, and the top decay products, $b + 2j$, tend to go in the same direction. The jets that goes in the same direction are efficiently picked up by the hemisphere method. In the analysis therefore we require all $b + 2j$ are in the same hemisphere.

Since there are a large number of jets in SUSY events, the combinatorial background for W reconstruction still remains after the restriction. In order to estimate the back-

[7] This event topology is essentially the same as in the focus point like region [74]. However in our scenario the branching ratio to the $4b + 4W + \not{E}_T$ final states is very large because gluino can decay to the 3rd generation squarks in 2-body way.

JHEP10(2009)005

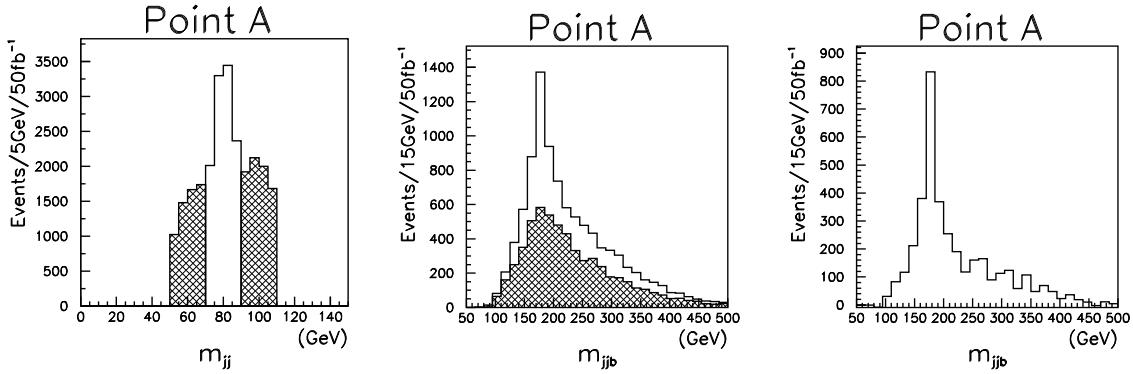

Figure 13. **Left;** The invariant mass distribution of the jet pairs that give the closest value to $m_{jj} = m_W - 20\,\mathrm{GeV}$ for sideband region I, $m_{jj} = m_W$ for W mass region, $m_{jj} = m_W + 20\,\mathrm{GeV}$ for sideband region II. **Center;** The invariant mass distributions of jjb, where the jet pair is in the W mass region. The shaded region represents the estimated background distribution from the fake W jet pairs. The background is estimated from events in the sideband region I and II by rescaling the momenta and normalizing the number of events events. **Right;** The jjb invariant mass distribution after the background subtraction.

ground distribution from fake jet pairs whose invariant mass is $\sim m_W$, we apply sideband subtractions [19, 75]. We first define the W mass region and sideband regions as follows,

$$\begin{aligned} |m_{jj} - m_W| &\leq 10\,\mathrm{GeV} \quad \cdots \quad (W \text{ mass region}), \\ |m_{jj} - (m_W - 20\,\mathrm{GeV})| &< 10\,\mathrm{GeV} \quad \cdots \quad (W \text{ sideband region I}), \\ |m_{jj} - (m_W + 20\,\mathrm{GeV})| &< 10\,\mathrm{GeV} \quad \cdots \quad (W \text{ sideband region II}). \end{aligned} \tag{5.13}$$

If the event contains several jet pairs in the same region, we choose the jet pair whose invariant mass is the closest to m_W for W mass region and to $m_W \mp 20\,\mathrm{GeV}$ for sideband region I (II), respectively.[8] In figure 13 (left) we show the selected two jets invariant mass distributions. The number of events in W mass region is clearly bigger than those in the sideband regions.

The central figure shows the jjb invariant mass distributions, where the two jets are the closest jet pair to m_W. Here the open histogram shows the distribution of the events in W mass region. On the other hand, the shaded distribution shows the background estimated from the sideband events. Namely, the jet pair momentum in region I (II) is rescaled by a factor $(m_W/(m_W \mp 20\,\mathrm{GeV}))$ before calculating m_{jjb}, and the two distributions are averaged. The right figure shows the $W + b$ invariant mass distribution after subtracting the sideband distribution. It has a clear peak at the top mass, which indicates that the SUSY events contain top quarks with a significant rate.

Because we find very prominent top quarks, it is natural to think tb distribution also show the clear kinematical structure. At pont A, the dominant gluino cascade decay chain is $\widetilde{g} \to \widetilde{t}_1 t \to \chi_1^{\pm} bt$ with 47% of the branching ratio. The m_{tb} distribution should have an

[8]The events may be double counted in the different regions.

JHEP10(2009)005

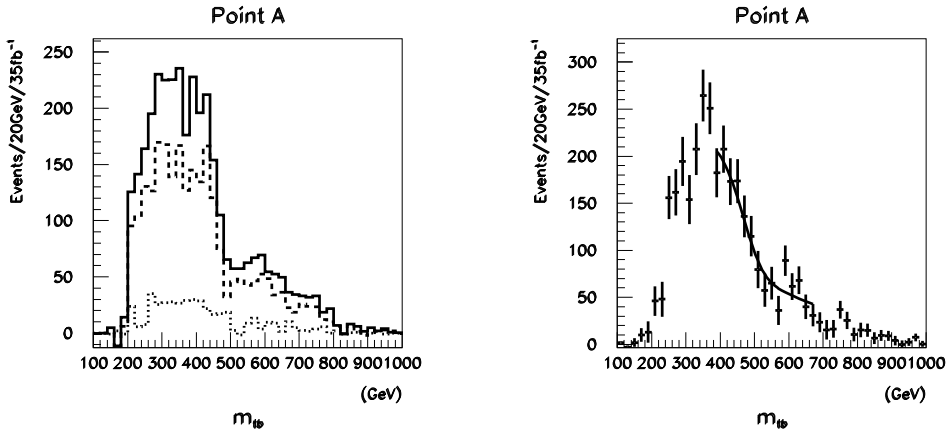

Figure 14. The Wbj invariant mass distribution after the W sideband subtraction. The left (right) figure is a result of parton (jet) level analysis.

edge. The kinematical maximum of the tb invariant mass is given as

$$m_{tb}^{\max} = \left(m_t^2 + \frac{m_{\tilde{t}_1}^2 - m_{\tilde{\chi}_1^\pm}^2}{2m_{\tilde{t}_1}^2} \left[(m_{\tilde{g}}^2 - m_{\tilde{t}_1}^2 - m_t^2) + \sqrt{(m_{\tilde{g}}^2 - m_{\tilde{t}_1}^2 - m_t^2)^2 - 4m_{\tilde{t}_1}^2 m_t^2} \right] \right)^{1/2}$$
$$= 475\,\mathrm{GeV}\ . \tag{5.14}$$

However searching the endpoint in a tagged tb distribution is not successful. This is because there are typically 4 b partons in the final state. When an event has 2 tagged b jets in the final state and one of the jjb system has a mass consistent with top mass, the probability that the other b jets is coming from the same gluino cascade decay chain is only 1/3. In addition, the probability that both the two b tagged jets are satisfy the hemisphere cut $p_T > 50\,\mathrm{GeV}$ and $|\eta| < 2.5$ is not large. One would also loose events by requiring $m(bW) \sim m_t$.

Instead, we study the Wbj distirbution. The W is selected by the sideband method, while one of the other two jets in the same hemisphere is tagged as b. The other jet is the highest jet in the hemisphere except for the used jets. When there are more than one b tagged jets in a hemisphere, we take the highest p_T b jet.

We show the Wbj invariant mass distributions after the W sideband subtraction in figure 14. The left figure shows the result of a parton level analysis. Here the parton momenta from cascade decays are taken from HERWIG event record and they are processed by the same hemishpere algorithm. We assume 60% tagging efficiency for b quark. The total distribution has a clear endpoint of the cascade decay, $\tilde{g} \to \tilde{t}_1 t \to \chi_1^\pm bt$, expected at 475 GeV. The contribution of the events where at least one gluino decays though the decay chain (a) is shown by a dashed line in the figure. A dotted line represents the contribution from the events that contains subdominant decay chain (d), which does not show such structure at $\sim$ 475 GeV. The other gluino decay modes do not give statistically significant contributions.

JHEP10(2009)005

The jet level distribution is shown in figure 14 (right). The distribution is smeared due to the jet energy resolution. Note that this is a distribution of 4 jet system, where two of the jets are from b parton. Nevertheless, the endpoint structure is still visible. We fit the fitting function used in ref. [75] to the distribution. The fitted endpoint is at $468 \pm 7\,\mathrm{GeV}$, which is consistent with the theoretically expected value 475 GeV. The significant edge proves the existence of the decay $\widetilde{g} \to \widetilde{t}_1 t \to \widetilde{\chi}_1^{\pm} tb$.

5.2 Inclusive M_{T2} and $M_{T2}^{\min}$ distributions

Recently, it is realized that M_{T2} variable is useful to determine the squark and gluino masses at the LHC [32, 33]. The M_{T2} variable is defined for a system of sparticle pair production and decay, namely the system with two visible objects $\mathbf{p}_{T1}^{\mathrm{vis}}$ and $\mathbf{p}_{T2}^{\mathrm{vis}}$ and missing momentum arising from 2 LSPs $\not{p}_T = \mathbf{p}_T^{\mathrm{LSP1}} + \mathbf{p}_{T2}^{\mathrm{LSP2}}$, as a function of an arbitrary test LSP mass m_χ, as follows:

$$M_{T2}(m_\chi) = \min_{\mathbf{p}_{T1}^{\mathrm{miss}} + \mathbf{p}_{T2}^{\mathrm{miss}} = \not{p}_T} \left[\max\{ m_T^{(1)}(\mathbf{p}_{T1}^{\mathrm{vis}}, \mathbf{p}_{T1}^{\mathrm{miss}}), m_T^{(2)}(\mathbf{p}_{T2}^{\mathrm{vis}}, \mathbf{p}_{T2}^{\mathrm{miss}}) \} \right], \tag{5.15}$$

The minimization is taken for the test LSP momenta, $\mathbf{p}_{T1}^{\mathrm{miss}}$ and $\mathbf{p}_{T2}^{\mathrm{miss}}$, under the constraint $\mathbf{p}_{T1}^{\mathrm{miss}} + \mathbf{p}_{T2}^{\mathrm{miss}} = \not{p}_T$. The transverse mass, $m_T^{(i)}$, is defined as

$$[m_T^{(i)}(\mathbf{p}_{Ti}^{\mathrm{vis}}, \mathbf{p}_{Ti}^{\mathrm{miss}})]^2 = (m_i^{\mathrm{vis}})^2 + m_\chi^2 + 2(E_{Ti}^{\mathrm{vis}} E_{Ti}^{\mathrm{miss}} - \mathbf{p}_{Ti}^{\mathrm{vis}} \cdot \mathbf{p}_{Ti}^{\mathrm{miss}}), \tag{5.16}$$

where m_i^{vis} is the invariant mass of the "visible object", $(m_i^{\mathrm{vis}})^2 = (p_i^{\mathrm{vis}})^2$ and $E_{Ti} = \sqrt{\mathbf{p}_{Ti}^2 + m_\chi^2}$. The kinematical upper bound of the transverse mass $m_T^{(i)}$ is given by the mother particle mass if $\mathbf{p}_{Ti}^{\mathrm{miss}} = \mathbf{p}_T^{\mathrm{LSP}i}$ and $m_\chi = m_{\widetilde{\chi}_1^0}$. Because of this property the kinematical upper bound of the M_{T2} variable is given by

$$M_{T2}(m_{\widetilde{\chi}_1^0}) \leq \max\{m_1, m_2\}, \tag{5.17}$$

where m_1 and m_2 are masses of the initially produced sparticles. Thus, the endpoint of the M_{T2} distribution relates to the heavy squark mass in our scenario as:

$$M_{T2}^{\mathrm{end}}(m_{\widetilde{\chi}_1^0}) \sim m_{\widetilde{q}}. \tag{5.18}$$

Squark and gluino production events often produce $\mathcal{O}(10)$ jets in the final state. The central question for the application of M_{T2} analysis is how to define the $\mathbf{p}_{Ti}^{\mathrm{vis}}$ in such cases. The "inclusive M_{T2}" is defined so that $\mathbf{p}_{Ti}^{\mathrm{vis}}$ is taken as a hemisphere momentum in eq. (5.10). In addition, a sub-sytem M_{T2} is introduced in refs. [33, 34] which is defined as an inclusive M_{T2} but the highest p_T jet is removed before hemisphere reconstruction. As discussed in the previous section, a quark jet from the decay $\widetilde{q} \to q\widetilde{g}$ or $\widetilde{q} \to q\widetilde{\chi}_i$ tends to be the highest p_T jet if $m_{\widetilde{q}} \gg m_{\widetilde{g}}$, which is also the case for our scenario (See eq. (3.2)). The sub-system after removing the highest jet tends to be $\widetilde{g}$-$\widetilde{g}$ or $\widetilde{g}$-$\widetilde{\chi}_i$ system for $\widetilde{g}$-$\widetilde{q}$ production events. Thus the endpoint of the subsystem M_{T2} should be the gluino mass.

More systematical approach to observe the gluino mass is using the minimum M_{T2}. The minimum M_{T2} ($M_{T2}^{\min}$) is defined by

$$M_{T2}^{\min} = \min_{i=1,\ldots,5} \left[M_{T2}^{\mathrm{sub}}(i) \right], \tag{5.19}$$

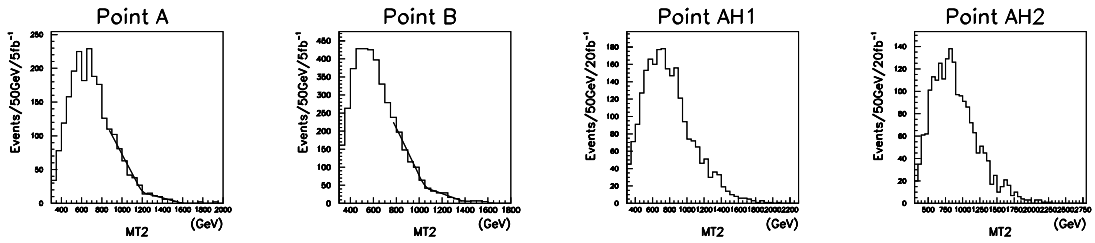

Figure 15. The inclusive M_{T2} distributions at Points A, B, AH1 and AH2. The result of the endpoint fit are $M_{T2}^{\rm end} = 1199 \pm 23$ and $1051 \pm 16\,{\rm GeV}$ for Point A and B, respectively. The first two generation squark masses are $m_{\widetilde{q}} \simeq 1150$ and $1080\,{\rm GeV}$ for Points A and B, respectively.

where $M_{T2}^{\rm sub}(i)$ is a generalized sub-system M_{T2} defined by removing the i-th high p_T jet before hemisphere reconstruction. The $M_{T2}^{\rm min}$ has been defined in ref. [36] for the leading 5 jets of the events $pp \to \widetilde{g}\widetilde{g} \to 4j + 2\widetilde{\chi}_1^0$ to reduce an effect of the initial state radiation (ISR) to a $\widetilde{g}$-$\widetilde{g}$ system. Namely, if a gluino pair is produced via a $gq \to \widetilde{g}\widetilde{g}j$ process, this jet may have a large p_T compared with some of jets from a sparticle cascade decay. By using $M_{T2}^{\rm min}$ one can effectively reduces the contamination from the ISR jet in $\widetilde{g}$-$\widetilde{g}$ production events.

In this paper, we use $M_{T2}^{\rm min}$ to reduce the additional jet from $\widetilde{q} \to q\widetilde{g}$ in $\widetilde{g}$-$\widetilde{q}$ events as well as the effect of the ISR jet in $\widetilde{g}$-$\widetilde{g}$ events. Note that for our model points, a gluino decay may lead 6 jets in the final state, therefore the chance that those jets are soft compared with the ISR is not small. The endpoint of the $M_{T2}^{\rm min}$ is given by the gluino mass:

$$(M_{T2}^{\rm min}(m_{\widetilde{\chi}_1^0}))^{\rm end} \sim m_{\widetilde{g}}. \tag{5.20}$$

We show the inclusive M_{T2} distributions of our sample model points in figure 15. Here we choose $m_\chi = 100\,{\rm GeV}$, and $p_{\rm vis}^{(1)} = p_{\rm hemi}^{(1)}$ and $p_{\rm vis}^{(2)} = p_{\rm hemi}^{(2)}$ for the M_{T2} calculation.[9] In addition to the standard SUSY cut, we require no isolated lepton, $p_T^{\rm jet} > 50\,{\rm GeV}$ and $|\eta^{\rm jet}| < 2.5$ for the jet involved in a hemisphere. We also require $N_{300}^{\rm jets} \geq 1$ for Points A and B, and $N_{400(600)}^{\rm jets} \geq 1$ for Point AH1 (AH2) to select $\widetilde{q}$-$\widetilde{g}(\widetilde{q})$ production events. We can optimize this cut from the difference of the $p_T^{(1)}$ distributions for b tagged and non-b tagged jets (See figures 5 and 6). The cross sections of squark productions are small for Points AH1 and AH2 (See table 3). We use events correspond to 20 fb^{-1} for Points AH1 and AH2, while 5 fb^{-1} for Points A and B.

The M_{T2} distributions at Point A and B have endpoints near the squark mass: $m_{\widetilde{q}} \simeq$ 1150 and 1080 for Points A and B, respectively. We fit the distributions by a simple fitting function

$$f(m) = \Theta(m - M_{T2}^{\rm end})[a_1(m - M_{T2}^{\rm end}) + b] + \Theta(M_{T2}^{\rm end} - m)[a_2(M_{T2}^{\rm end} - m) + b], \tag{5.21}$$

to see if the endpoints are recovered correctly. We obtain $M_{T2}^{\rm end} = 1199 \pm 23$ and $1051 \pm 16\,{\rm GeV}$ for Points A and B, respectively. They are roughly consistent with the input squark masses.

[9] We require p^1(seed) and p^2(seed) remain in the different hemispheres when we calculate M_{T2} and $M_{T2}^{\rm min}$. The condition seems important to keep the events near the endpoint of $M_{T2}^{\rm min}$.

JHEP10(2009)005

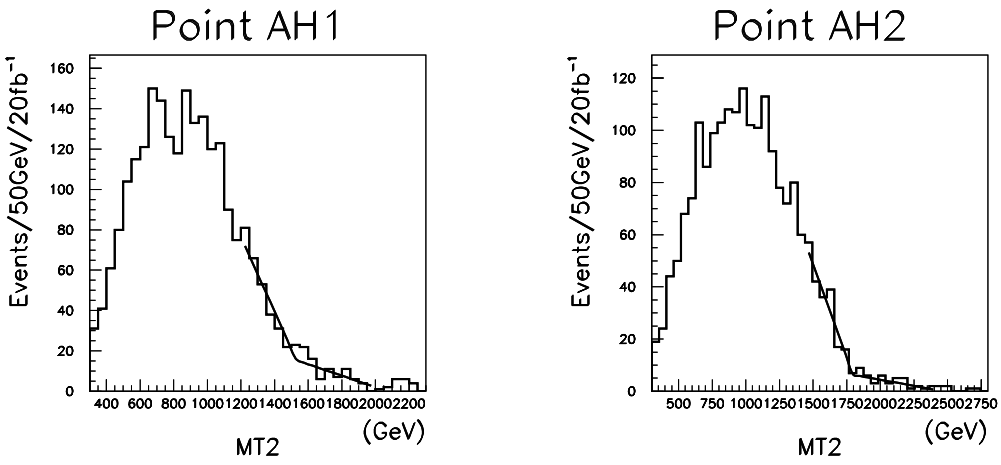

Figure 16. The distributions of the M_{T2} ($= \min\{M_{T2}^{(1)}, M_{T2}^{(2)}\}$) at AH1 and AH2. The results of the endpoint fit are $M_{T2}^{\rm end} = 1530 \pm 31$ and 1798 ± 21 GeV for Points AH1 and AH2, respectively. The first two generation squark masses are $m_{\widetilde{q}} \simeq 1500$ and 1780 GeV for Points AH1 and AH2, respectively.

For Points AH1 and AH2 (especially for AH2), there are a few events in the regions where $M_{T2} \lesssim m_{\widetilde{q}}$. At these model points, a half of the heavy squark mass is larger than the gluino mass, $m_{\widetilde{q}}/2 \gtrsim m_{\widetilde{g}}$. It is therefore expected that a gluino from the squark decay $\widetilde{q} \to \widetilde{g}q$ is boosted and goes in the opposite direction from the direction of the quark jet q. In that case, decay products of the $\widetilde{g}$ and the quark jet q are not likely to be in the same hemisphere.

To reconstruct the heavy squark mass, we should separate the final states of $\widetilde{g}$-$\widetilde{q} \to \widetilde{g}$-$\widetilde{g}$-$q$ events into three parts, two groups of decay products of the gluinos and the quark jet q. We adopt the same technique as that used in the sub-system M_{T2}. Namely, we remove the highest p_T jet in the event, and the rest of jets and leptons are grouped into the each hemisphere. Next we assign the highest p_T jet into one of the hemispheres and calculate M_{T2}. This gives two M_{T2} values, $M_{T2}^{(1)}$ and $M_{T2}^{(2)}$, depending on which hemisphere the quark jet is assigned. Finally, we choose the smaller $M_{T2}^{(i)}$, $M_{T2} = \min\{M_{T2}^{(1)}, M_{T2}^{(2)}\}$.

The distributions of the M_{T2} calculated from such procedure at Points AH1 and AH2 are shown in figure 16. Here we adopt the same cuts as in figure 15. The distributions have robust endpoint structures near the correct squark masses: 1500 and 1780 GeV for Points AH1 and AH2, respectively. We fit the distributions by the fitting function in eq. (5.21). The results are $M_{T2}^{\rm end} = 1530 \pm 31$ and 1798 ± 21 GeV for Points AH1 and AH2, respectively. They are consistent with the input squark masses.

Next, we show the $M_{T2}^{\rm min}$ distributions for Points A and B in figure 17.[10] Here, we require $N_{300}^{\rm jets} = 0$ to reduce the $\widetilde{q}$-$\widetilde{q}(\widetilde{g})$ production events. The numbers of events corresponds to $\int \mathcal{L} = 5$ fb^{-1} for each model points. We fit the $f(x)$ in eq. (5.21) to the $M_{T2}^{\rm min}$ distributions. We obtain $(M_{T2}^{\rm min})^{\rm end} = 715 \pm 14$ and 524 ± 8 GeV at Points A and B, respectively. They are roughly consistent with input gluino masses: $m_{\widetilde{g}} = 697$ and 544 GeV for Points

[10] We do not show the distributions for Points AH1 and AH2 because their gluino mass are almost the same as that of Point A.

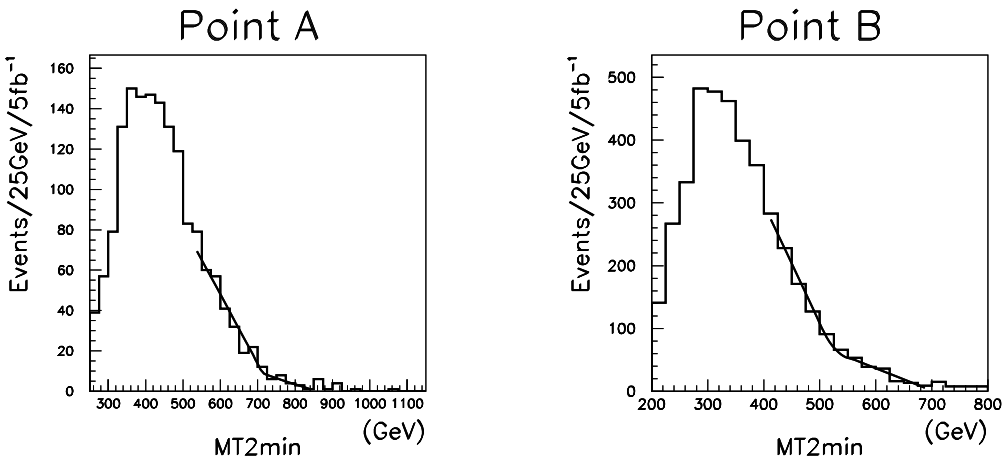

Figure 17. The $M_{T2}^{\min}$ distributions at Points A and B. The results of the endpoint fit are $(M_{T2}^{\min})^{\rm end} = 715 \pm 14$ and $524 \pm 8\,{\rm GeV}$ for Points A and B, respectively. The gluino masses are $m_{\widetilde{g}} \simeq 697$ and 544 GeV for Points A and B, respectively.

A and B, respectively.

If one assume GUT relation among the gaugino masses and gaugino dominance of the $\chi_1^\pm$, one can roughly estimate the $\chi_1^\pm$ mass from the gluino mass. Since the tb endpoint is a function of $m_{\widetilde{g}}$, $m_{\chi_1^\pm}$ and $m_{\widetilde{t}_1}$, one can get the information of $m_{\widetilde{t}_1}$ from the the measured gluino mass and the tb endpoint.

6 Summary and conclusion

In this paper, we investigate the LHC signature of modified universal sfermion mass (MUSM) scenario. In the scenario the sfermion mass matrices can be parametrized as in eq. (2.3) at the GUT scale. In this paper, we concentrate the region where $m_0 \gg m_{30}$, $m_{1/2}$, m_{H_u}, μ based on the considerations of naturalness and flavor and CP constraints.

In this scenario, gluino decays entirely into the 3rd generation squarks. The SUSY events typically have 4 b partons. The fraction of the SUSY events without b tagged jets is suppressed even if the b tagging efficiency is 60%. This is a feature of models with the mass relation eq. (3.1).

The 1st and 2nd generation squarks are much heavier than gluino and the 3rd generation squarks in this scenario. The mass of the heavy squarks m_0 cannot be arbitrarily large from CCB constraint. The heavy squarks can be observed at the LHC if $m_0 \lesssim 1 - 2\,{\rm TeV}$. A quark jet from the decay $\widetilde{q} \to \widetilde{g}q$ tends to have large p_T ($p_T \lesssim m_{\widetilde{q}}/2$), and they will be tagged as the excess of the non-b tagged jets in the high p_T range relative to the b tagged jets. The excess indicates the mass relation eq. (3.2).

The signature similar to that of MUSM scenario may be observed at some CMSSM points with $|A_0| > m_0 \gg m_{1/2}$. For MUSM scenario, gluino decay modes are $\widetilde{g} \to \widetilde{t}_1 t$ and

JHEP10(2009)005

$\widetilde{g} \to \widetilde{b}_1 b$, while gluino decay is dominated by $\widetilde{g} \to \widetilde{t}_1 t$ mode for the CMSSM region . This difference may be seen in the $\widetilde{\chi}_2^0 \to \widetilde{\chi}_1^0 Z$ channel. If a $\widetilde{\chi}_2^0$ is originated from the $\widetilde{b}_1$ decay, the number of associated jets is 2 ($b\bar{b}$). On the other hand if $\widetilde{\chi}_2^0$ is originated from the $\widetilde{t}_1$ decay, it is 6 ($b\bar{b} + 2W(jj)$) when both of the W bosons decay into jets. We demonstrate that we can discriminate these scenarios by investigating the number of jets in the event with 2 leptons with $m_{ll} \sim m_Z$.

In MUSM scenario, the events contain many jets arising from gluino decays. The mass reconstructions of the SUSY particles are challenging due to the combinatorial background. However, we find that successful reconstructions are possible. The conventional endpoint analysis with OSSF lepton pair from a cascade decay chain (5.4) is useful if $m_{1/2}$ and $|A_0|$ are small enough to satisfy conditions (5.3). We demonstrate that all sparticle masses arising from the decay chain (5.4) can be measured at the LHC in such case. On the other hand, if $m_{1/2}$ or $|A_0|$ is large enough, we have to use events without leptons for the exclusive analysis. We have succeeded to reduce the combinatorial background by searching for jet pair consistent with W in the same hemisphere. Especially we can efficiently reconstruct the top quark arising from gluino decays into scalar top. Moreover we demonstrate that the endpoint in the Wbj distribution can be seen even in the jet level analysis, which indicated the tb endpoint of the $\widetilde{g} \to \widetilde{t}_1 t \to \chi_1^{\pm} bt$ mode.

The inclusive M_{T2} and $M_{T2}^{\min}$ distribution is also useful for the mass determination of gluino and the heavy squarks. The squark mass can be measured from the endpoint of the M_{T2} distribution. Moreover we reconstruct the $\widetilde{g}$-$\widetilde{g}$ and/or $\widetilde{g}$-$\widetilde{\chi}_i$ "sub-system" by removing the i-th high p_T jet before hemisphere reconstruction and calculating subsystem M_{T2} called $M_{T2}^{\rm sub}(i)$. The gluino mass can be measured from the endpoint of the $M_{T2}^{\min}$ ($\equiv \min_{i=1}^{5} \left[M_{T2}^{\rm sub}(i)\right]$) distribution. By combining the measured gluino mass and tb endpoint, one can get the information of the stop mass only from the analysis using jets. Such inclusive analyses may tell us both the mass scales of squarks and gluino in the early stage of the LHC such as $\int \mathcal{L} \simeq 5 - 20$ fb^{-1}.

Acknowledgments

This work is supported by the World Premier International Research Cernter Initiative (WPI initiative) by MEXT, Japan. S.K, N.M and K.I.N are supported in part by Grants-in-Aid for Scientific Research from the Ministry of Education, Culture, Sports, Science and Technology of Japan.

A Masses and branching ratios

B Comparison with SPS benchmark points

For comparison of MUSM scenario with other scenarios with universal sfermion masses, we show the distribution of number of b tagged jet and the $p_T^{(1)}$ distributions at several benchmark model points called snowmass points and slopes (SPS) [70]. Here, the same cut as in section 3 is adopted. The number of generated events correspond to $\int \mathcal{L} dt = 1$ fb^{-1}.

particle	A	B	U
$\widetilde{g}$	697	537	707
$\widetilde{d}_L$	1152	1085	1150
$\widetilde{u}_L$	1150	1082	1147
$\widetilde{d}_R$	1143	1080	1142
$\widetilde{u}_R$	1144	1082	1142
$\widetilde{b}_1$	540	400	868
$\widetilde{t}_1$	321	296	484
$\widetilde{b}_2$	1129	1069	1077
$\widetilde{t}_2$	612	475	896
$\widetilde{e}_L$	1016	1010	1015
$\widetilde{e}_R$	1005	1000	1005
$\widetilde{\nu}_e$	1013	1007	1012
$\widetilde{\tau}_1$	298	183	932
$\widetilde{\tau}_2$	1013	1007	987
$\widetilde{\nu}_\tau$	1011	1006	979
$\widetilde{\chi}_1^0$	110	77	113
$\widetilde{\chi}_2^0$	210	138	221
$\widetilde{\chi}_3^0$	470	258	742
$\widetilde{\chi}_4^0$	486	289	748
$\widetilde{\chi}_1^+$	211	137	221
$\widetilde{\chi}_2^+$	486	287	750
h^0	115	100	119
H^0	560	115	1153
A^0	557	105	1146
$H^\pm$	567	135	1157

mode		BR(%)		
		A	B	U
$\widetilde{u}_L$	$\to \widetilde{g}u$	67	74	66
	$\to \widetilde{\chi}_1^+ d$	21	15	22
	$\to \widetilde{\chi}_2^0 u$	10	7	11
$\widetilde{d}_L$	$\to \widetilde{g}d$	68	74	67
	$\to \widetilde{\chi}_1^- u$	20	12	22
	$\to \widetilde{\chi}_2^0 d$	10	6	11
$\widetilde{u}_R$	$\to \widetilde{g}u$	92	94	91
	$\to \widetilde{\chi}_1^0 u$	8	6	9
$\widetilde{d}_R$	$\to \widetilde{g}d$	98	98	98
	$\to \widetilde{\chi}_1^0 d$	2	2	2
$\widetilde{g}$	$\to \widetilde{t}_1 \bar{t}\,(\widetilde{t}_1^* t)$	64	30	100
	$\to \widetilde{b}_1 \bar{b}\,(\widetilde{b}_1^* b)$	36	70	0
$\widetilde{t}_1$	$\to \widetilde{\chi}_1^+ b$	73	91	30
	$\to \widetilde{\chi}_2^0 t$	0	0	9
	$\to \widetilde{\chi}_1^0 t$	27	9	61
$\widetilde{b}_1$	$\to \widetilde{t}_1 W^-$	63	15	41
	$\to \widetilde{\chi}_1^- t$	20	35	22
	$\to \widetilde{\chi}_2^0 b$	16	39	12
	$\to \widetilde{\chi}_1^0 b$	1	6	1
	$\to \widetilde{g}b$	0	0	24
$\widetilde{\chi}_1^-$	$\to \widetilde{\chi}_1^0 W^-$	100	0	100
	$\to \widetilde{\chi}_1^0 \bar{u}d$	0	67	0
	$\to \widetilde{\chi}_1^0 l^- \bar{\nu}_l$	0	22	0
	$\to \widetilde{\chi}_1^0 \tau^- \bar{\nu}_\tau$	0	11	0
$\widetilde{\chi}_2^0$	$\to \widetilde{\chi}_1^0 Z^0$	100	0	100
	$\to \widetilde{\chi}_1^0 u\bar{u}(d\bar{d})$	0	24	0
	$\to \widetilde{\chi}_1^0 b\bar{b}$	0	31	0
	$\to \widetilde{\chi}_1^0 l^+ l^-$	0	5	0
	$\to \widetilde{\chi}_1^0 \tau^+ \tau^-$	0	6	0
	$\to \widetilde{\chi}_1^0 \nu\bar{\nu}$	0	15	0

Table 4. **Left;** Mass spectra of sparticles and Higgs bosons for our model points in GeV. **Right;** Branching ratios of sparticles for our model points. Here, u and d denote both the first and the second generation up and down type quarks, respectively

JHEP10(2009)005

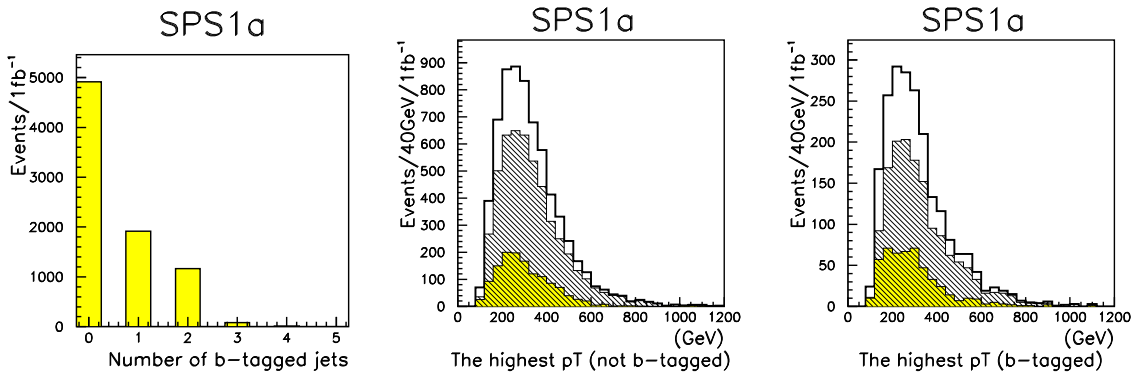

Figure 18. **SPS1a** (Typical point); $m_0 = 100\,\text{GeV}$, $m_{1/2} = 250\,\text{GeV}$, $A_0 = -100\,\text{GeV}$, $\tan\beta = 10$, $\text{sgn}(\mu) = +$.

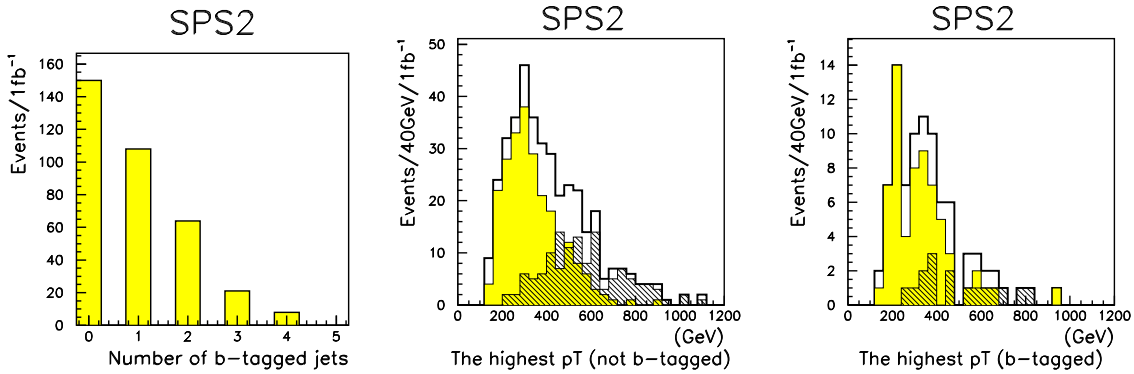

Figure 19. **SPS2** (Focus point); $m_0 = 1450\,\text{GeV}$, $m_{1/2} = 300\,\text{GeV}$, $A_0 = 0\,\text{GeV}$, $\tan\beta = 10$, $\text{sgn}(\mu) = +$.

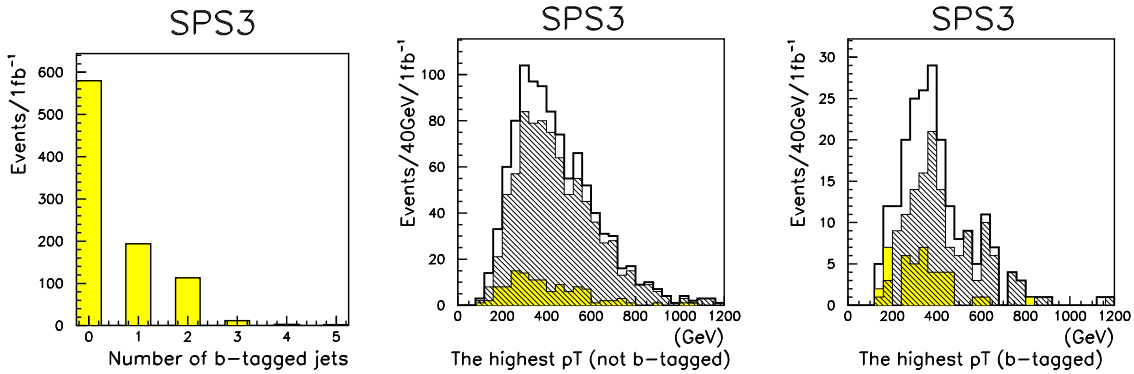

Figure 20. **SPS3** (Coannihilation region); $m_0 = 90\,\text{GeV}$, $m_{1/2} = 400\,\text{GeV}$, $A_0 = 0\,\text{GeV}$, $\tan\beta = 10$, $\text{sgn}(\mu) = +$

JHEP10(2009)005

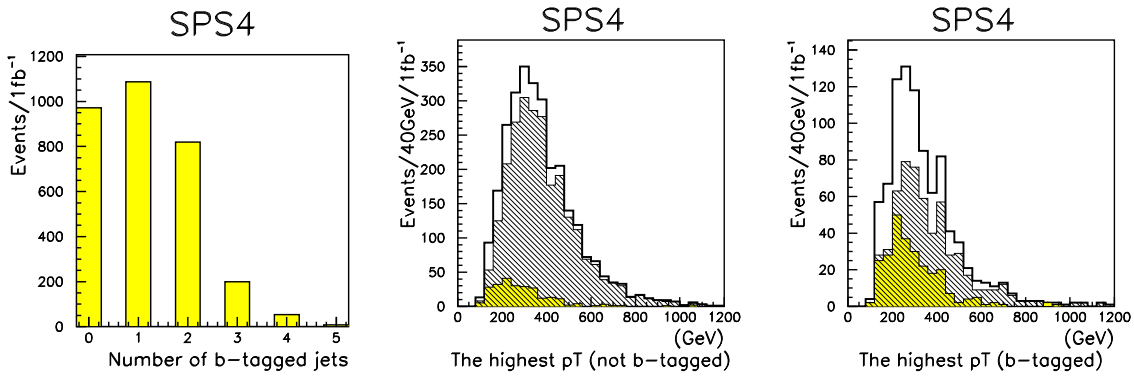

Figure 21. **SPS4** (Large $\tan\beta$); $m_0 = 400\,\text{GeV}$, $m_{1/2} = 300\,\text{GeV}$, $A_0 = 0\,\text{GeV}$, $\tan\beta = 50$, $\text{sgn}(\mu) = +$

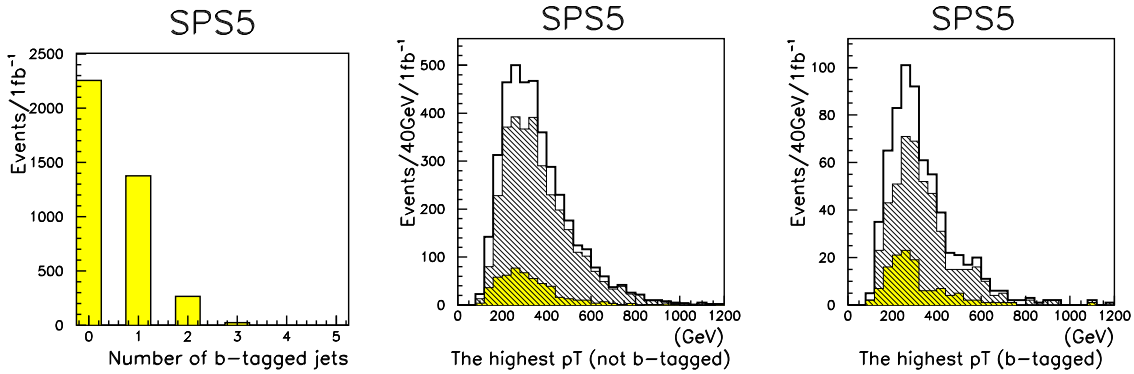

Figure 22. **SPS5** (Light stop); $m_0 = 150\,\text{GeV}$, $m_{1/2} = 300\,\text{GeV}$, $A_0 = -1000\,\text{GeV}$, $\tan\beta = 5$, $\text{sgn}(\mu) = +$

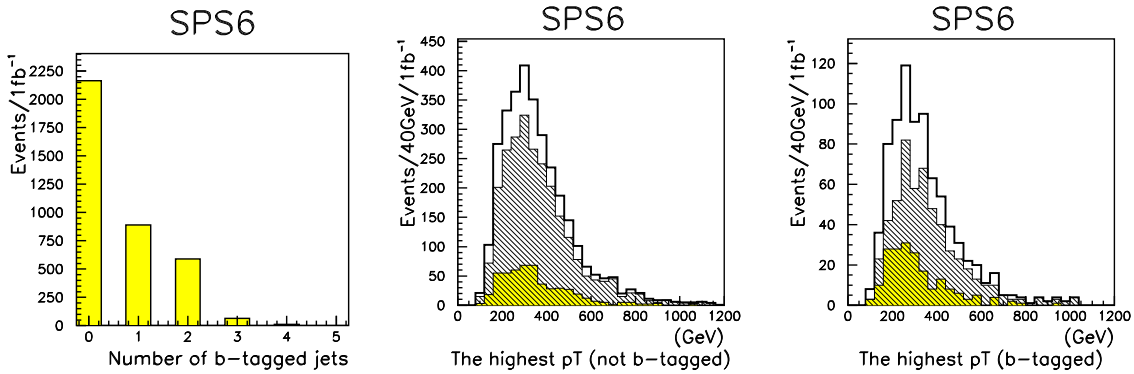

Figure 23. **SPS6** (Non-universal gaugino); $m_0 = 150\,\text{GeV}$, $M_1 = 480\,\text{GeV}$, $M_2 = M_3 = 300\,\text{GeV}$, $A_0 = 0\,\text{GeV}$, $\tan\beta = 10$, $\text{sgn}(\mu) = +$

JHEP10(2009)005

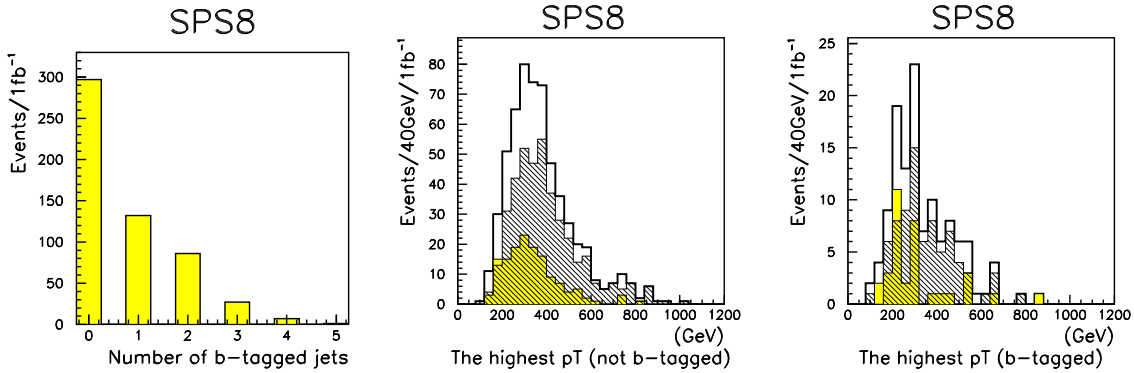

Figure 24. **SPS8** (GMSB scenario); $\Lambda = 40\,\text{TeV}$, $M_{mess} = 80\,\text{TeV}$, $N_{mess} = 1$, $\tan\beta = 15$, $\text{sgn}(\mu) = +$

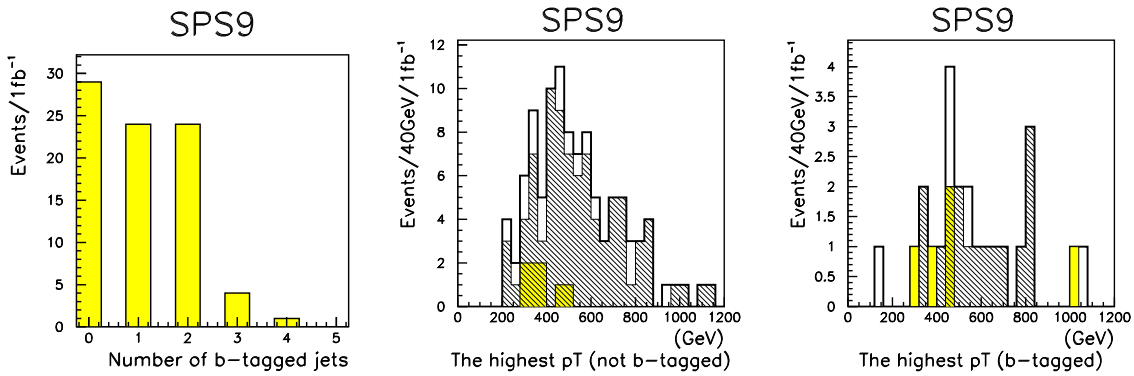

Figure 25. **SPS9** (AMSB scenario); $m_0 = 400\,\text{GeV}$, $m_{3/2} = 60\,\text{TeV}$, $\tan\beta = 10$, $\text{sgn}(\mu) = +$

JHEP10(2009)005

References

[1] H.P. Nilles, *Supersymmetry, supergravity and particle physics*, *Phys. Rept.* **110** (1984) 1 [SPIRES].

[2] H.E. Haber and G.L. Kane, *The search for supersymmetry: probing physics beyond the Standard Model*, *Phys. Rept.* **117** (1985) 75 [SPIRES].

[3] S.P. Martin, *A supersymmetry primer*, hep-ph/9709356 [SPIRES].

[4] I. Hinchliffe, F.E. Paige, M.D. Shapiro, J. Soderqvist and W. Yao, *Precision SUSY measurements at CERN LHC*, *Phys. Rev.* **D 55** (1997) 5520 [hep-ph/9610544] [SPIRES].

[5] I. Hinchliffe and F.E. Paige, *Measurements in SUGRA models with large* $\tan\beta$ *at LHC*, *Phys. Rev.* **D 61** (2000) 095011 [hep-ph/9907519] [SPIRES].

[6] H. Bachacou, I. Hinchliffe and F.E. Paige, *Measurements of masses in SUGRA models at CERN LHC*, *Phys. Rev.* **D 62** (2000) 015009 [hep-ph/9907518] [SPIRES].

[7] B.C. Allanach, C.G. Lester, M.A. Parker and B.R. Webber, *Measuring sparticle masses in non-universal string inspired models at the LHC*, *JHEP* **09** (2000) 004 [hep-ph/0007009] [SPIRES].

[8] J.L. Feng and T. Moroi, *Tevatron signatures of longlived charged sleptons in gauge mediated supersymmetry breaking models*, *Phys. Rev.* **D 58** (1998) 035001 [hep-ph/9712499] [SPIRES].

[9] I. Hinchliffe and F.E. Paige, *Measurements in gauge mediated SUSY breaking models at LHC*, *Phys. Rev.* **D 60** (1999) 095002 [hep-ph/9812233] [SPIRES].

[10] K. Kawagoe, T. Kobayashi, M.M. Nojiri and A. Ochi, *Study of the gauge mediation signal with non-pointing photons at the CERN LHC*, *Phys. Rev.* **D 69** (2004) 035003 [hep-ph/0309031] [SPIRES].

[11] F.E. Paige and J.D. Wells, *Anomaly mediated SUSY breaking at the LHC*, hep-ph/0001249 [SPIRES].

[12] A.J. Barr, C.G. Lester, M.A. Parker, B.C. Allanach and P. Richardson, *Discovering anomaly-mediated supersymmetry at the LHC*, *JHEP* **03** (2003) 045 [hep-ph/0208214] [SPIRES].

[13] A. Datta and K. Huitu, *Characteristic slepton signal in anomaly mediated SUSY breaking models via gauge boson fusion at the LHC*, *Phys. Rev.* **D 67** (2003) 115006 [hep-ph/0211319] [SPIRES].

[14] S. Asai, T. Moroi, K. Nishihara and T.T. Yanagida, *Testing the anomaly mediation at the LHC*, *Phys. Lett.* **B 653** (2007) 81 [arXiv:0705.3086] [SPIRES].

[15] S. Asai, T. Moroi and T.T. Yanagida, *Test of anomaly mediation at the LHC*, *Phys. Lett.* **B 664** (2008) 185 [arXiv:0802.3725] [SPIRES].

[16] H. Baer, E.-K. Park, X. Tata and T.T. Wang, *Measuring modular weights in mirage unification models at the LHC and ILC*, *Phys. Lett.* **B 641** (2006) 447 [hep-ph/0607085] [SPIRES].

[17] W.S. Cho, Y.G. Kim, K.Y. Lee, C.B. Park and Y. Shimizu, *LHC signature of mirage mediation*, *JHEP* **04** (2007) 054 [hep-ph/0703163] [SPIRES].

[18] CMS collaboration, S. Abdullin et al., *Discovery potential for supersymmetry in CMS*, *J. Phys.* **G 28** (2002) 469 [hep-ph/9806366] [SPIRES].

[19] ATLAS collaboration, *ATLAS detector and physic performance technical design report*, volume 1, CERN-LHCC-99-14, Cern Switzerland (1999) [SPIRES]; *ATLAS detector and physic performance technical design report*, volume 2, CERN-LHCC-99-15, Cern Switzerland (1999) [SPIRES].

[20] B.K. Gjelsten, . Miller, D. J. and P. Osland, *Measurement of SUSY masses via cascade decays for SPS* 1a, *JHEP* **12** (2004) 003 [hep-ph/0410303] [SPIRES].

[21] D.J. Miller, P. Osland and A.R. Raklev, *Invariant mass distributions in cascade decays*, *JHEP* **03** (2006) 034 [hep-ph/0510356] [SPIRES].

[22] B.K. Gjelsten, D.J. Miller, P. Osland and A.R. Raklev, *Mass determination in cascade decays using shape formulas*, *AIP Conf. Proc.* **903** (2007) 257 [hep-ph/0611259] [SPIRES].

[23] M.M. Nojiri, G. Polesello and D.R. Tovey, *Proposal for a new reconstruction technique for SUSY processes at the LHC*, hep-ph/0312317 [SPIRES].

[24] K. Kawagoe, M.M. Nojiri and G. Polesello, *A new SUSY mass reconstruction method at the CERN LHC*, *Phys. Rev.* **D 71** (2005) 035008 [hep-ph/0410160] [SPIRES].

JHEP10(2009)005

[25] M.M. Nojiri, G. Polesello and D.R. Tovey, *A hybrid method for determining SUSY particle masses at the LHC with fully identified cascade decays*, *JHEP* **05** (2008) 014 [arXiv:0712.2718] [SPIRES].

[26] H.-C. Cheng, D. Engelhardt, J.F. Gunion, Z. Han and B. McElrath, *Accurate mass determinations in decay chains with missing energy*, *Phys. Rev. Lett.* **100** (2008) 252001 [arXiv:0802.4290] [SPIRES].

[27] C.G. Lester and D.J. Summers, *Measuring masses of semiinvisibly decaying particles pair produced at hadron colliders*, *Phys. Lett.* **B 463** (1999) 99 [hep-ph/9906349] [SPIRES].

[28] A. Barr, C. Lester and P. Stephens, *m_{T2}: the truth behind the glamour*, *J. Phys.* **G 29** (2003) 2343 [hep-ph/0304226] [SPIRES].

[29] W.S. Cho, K. Choi, Y.G. Kim and C.B. Park, *Gluino stransverse mass*, *Phys. Rev. Lett.* **100** (2008) 171801 [arXiv:0709.0288] [SPIRES].

[30] A.J. Barr, B. Gripaios and C.G. Lester, *Weighing Wimps with kinks at colliders: invisible particle mass measurements from endpoints*, *JHEP* **02** (2008) 014 [arXiv:0711.4008] [SPIRES].

[31] W.S. Cho, K. Choi, Y.G. Kim and C.B. Park, *Measuring superparticle masses at hadron collider using the transverse mass kink*, *JHEP* **02** (2008) 035 [arXiv:0711.4526] [SPIRES].

[32] M.M. Nojiri, Y. Shimizu, S. Okada and K. Kawagoe, *Inclusive transverse mass analysis for squark and gluino mass determination*, *JHEP* **06** (2008) 035 [arXiv:0802.2412] [SPIRES].

[33] M.M. Nojiri, K. Sakurai, Y. Shimizu and M. Takeuchi, *Handling jets + missing E_T channel using inclusive m_{T2}*, *JHEP* **10** (2008) 100 [arXiv:0808.1094] [SPIRES].

[34] M. Burns, K. Kong, K.T. Matchev and M. Park, *Using subsystem m_{T2} for complete mass determinations in decay chains with missing energy at hadron colliders*, *JHEP* **03** (2009) 143 [arXiv:0810.5576] [SPIRES].

[35] W.S. Cho, K. Choi, Y.G. Kim and C.B. Park, *m_{T2}-assisted on-shell reconstruction of missing momenta and its application to spin measurement at the LHC*, *Phys. Rev.* **D 79** (2009) 031701 [arXiv:0810.4853] [SPIRES].

[36] J. Alwall, K. Hiramatsu, M.M. Nojiri and Y. Shimizu, *Novel reconstruction technique for new physics processes with initial state radiation*, arXiv:0905.1201 [SPIRES].

[37] S.I. Bityukov and N.V. Krasnikov, *The LHC (CMS) discovery potential for models with effective supersymmetry and nonuniversal gaugino masses*, *Phys. Atom. Nucl.* **65** (2002) 1341 [*Yad. Fiz.* **65** (2002) 1374] [hep-ph/0102179] [SPIRES].

[38] S. Bhattacharya, A. Datta and B. Mukhopadhyaya, *Non-universal scalar masses: a signal-based analysis for the Large Hadron Collider*, *Phys. Rev.* **D 78** (2008) 035011 [arXiv:0804.4051] [SPIRES]; *Non-universal gaugino and scalar masses, hadronically quiet trileptons and the Large Hadron Collider*, *Phys. Rev.* **D 78** (2008) 115018 [arXiv:0809.2012] [SPIRES].

[39] R. Barbieri and D. Pappadopulo, *S-particles at their naturalness limits*, arXiv:0906.4546 [SPIRES].

[40] J.R. Ellis and D.V. Nanopoulos, *Flavor changing neutral interactions in broken supersymmetric theories*, *Phys. Lett.* **B 110** (1982) 44 [SPIRES].

JHEP10(2009)005

[41] R. Barbieri and R. Gatto, *Conservation laws for neutral currents in spontaneously broken supersymmetric theories*, *Phys. Lett.* **B 110** (1982) 211 [SPIRES].

[42] J.S. Hagelin, S. Kelley and T. Tanaka, *Supersymmetric flavor changing neutral currents: exact amplitudes and phenomenological analysis*, *Nucl. Phys.* **B 415** (1994) 293 [SPIRES].

[43] F. Gabbiani, E. Gabrielli, A. Masiero and L. Silvestrini, *A complete analysis of FCNC and CP constraints in general SUSY extensions of the standard model*, *Nucl. Phys.* **B 477** (1996) 321 [hep-ph/9604387] [SPIRES].

[44] S. Dimopoulos and G.F. Giudice, *Naturalness constraints in supersymmetric theories with nonuniversal soft terms*, *Phys. Lett.* **B 357** (1995) 573 [hep-ph/9507282] [SPIRES].

[45] A. Pomarol and D. Tommasini, *Horizontal symmetries for the supersymmetric flavor problem*, *Nucl. Phys.* **B 466** (1996) 3 [hep-ph/9507462] [SPIRES].

[46] A.G. Cohen, D.B. Kaplan and A.E. Nelson, *The more minimal supersymmetric Standard Model*, *Phys. Lett.* **B 388** (1996) 588 [hep-ph/9607394] [SPIRES].

[47] S.G. Kim, N. Maekawa, A. Matsuzaki, K. Sakurai and T. Yoshikawa, *Lepton flavor violation in SUSY GUT model with non-universal sfermion masses*, *Phys. Rev.* **D 75** (2007) 115008 [hep-ph/0612370] [SPIRES].

[48] S.G. Kim, N. Maekawa, A. Matsuzaki, K. Sakurai and T. Yoshikawa, *CP asymmetries of $B \to \phi K_S$ and $B \to \eta' K_S$ in SUSY GUT model with non-universal sfermion masses*, *Prog. Theor. Phys.* **121** (2009) 49 [arXiv:0803.4250] [SPIRES].

[49] M. Ishiduki, S.G. Kim, N. Maekawa and K. Sakurai, *CEDM constraints on modified sfermion universality and spontaneous CP-violation*, arXiv:0901.3400 [SPIRES].

[50] N. Maekawa, *Non-abelian horizontal symmetry and anomalous* U(1) *symmetry for supersymmetric flavor problem*, *Phys. Lett.* **B 561** (2003) 273 [hep-ph/0212141] [SPIRES]; *E_6 unification, large neutrino mixings and SUSY flavor problem*, *Prog. Theor. Phys.* **112** (2004) 639 [hep-ph/0402224] [SPIRES].

[51] N. Maekawa and T. Yamashita, *Horizontal symmetry in Higgs sector of GUT with* $\mathrm{U}(1)_A$ *symmetry*, *JHEP* **07** (2004) 009 [hep-ph/0404020] [SPIRES].

[52] J.R. Ellis, T. Falk, G. Ganis, K.A. Olive and M. Srednicki, *The CMSSM parameter space at large* $\tan\beta$, *Phys. Lett.* **B 510** (2001) 236 [hep-ph/0102098] [SPIRES]; L. Roszkowski, R. Ruiz de Austri and T. Nihei, *New cosmological and experimental constraints on the CMSSM*, *JHEP* **08** (2001) 024 [hep-ph/0106334] [SPIRES]; J.R. Ellis, K.A. Olive and Y. Santoso, *Constraining supersymmetry*, *New J. Phys.* **4** (2002) 32 [hep-ph/0202110] [SPIRES].

[53] R. Dermisek, H.D. Kim and I.-W. Kim, *Mediation of supersymmetry breaking in gauge messenger models*, *JHEP* **10** (2006) 001 [hep-ph/0607169] [SPIRES].

[54] K. Hagiwara, A.D. Martin, D. Nomura and T. Teubner, *Improved predictions for g-2 of the muon and* $\alpha_{\rm QED}(M_Z^2)$, *Phys. Lett.* **B 649** (2007) 173 [hep-ph/0611102] [SPIRES].

[55] N. Arkani-Hamed and H. Murayama, *Can the supersymmetric flavor problem decouple?*, *Phys. Rev.* **D 56** (1997) 6733 [hep-ph/9703259] [SPIRES]; K. Agashe and M. Graesser, *Supersymmetry breaking and the supersymmetric flavour problem: an analysis of decoupling the first two generation scalars*, *Phys. Rev.* **D 59** (1999) 015007 [hep-ph/9801446] [SPIRES].

JHEP10(2009)005

[56] F.E. Paige, S.D. Protopopescu, H. Baer and X. Tata, *ISAJET 7.69: a Monte Carlo event generator for pp, $\bar{p}p$ and e^+e^- reactions*, hep-ph/0312045 [SPIRES].

[57] LEP Working Group for Higgs boson searches collaboration, R. Barate et al., *Search for the standard model Higgs boson at LEP*, *Phys. Lett.* **B 565** (2003) 61 [hep-ex/0306033] [SPIRES].

[58] Particle Data Group collaboration, C. Amsler et al., *Review of particle physics*, *Phys. Lett.* **B 667** (2008) 1 [SPIRES].

[59] Y. Okada, M. Yamaguchi and T. Yanagida, *Upper bound of the lightest Higgs boson mass in the minimal supersymmetric Standard Model*, *Prog. Theor. Phys.* **85** (1991) 1 [SPIRES]; *Renormalization group analysis on the Higgs mass in the softly broken supersymmetric standard model*, *Phys. Lett.* **B 262** (1991) 54 [SPIRES];
J.R. Ellis, G. Ridolfi and F. Zwirner, *Radiative corrections to the masses of supersymmetric Higgs bosons*, *Phys. Lett.* **B 257** (1991) 83 [SPIRES]; *On radiative corrections to supersymmetric Higgs boson masses and their implications for LEP searches*, *Phys. Lett.* **B 262** (1991) 477 [SPIRES];
A. Brignole, J.R. Ellis, G. Ridolfi and F. Zwirner, *The supersymmetric charged Higgs boson mass and LEP phenomenology*, *Phys. Lett.* **B 271** (1991) 123 [SPIRES];
H.E. Haber and R. Hempfling, *Can the mass of the lightest Higgs boson of the minimal supersymmetric model be larger than $m(Z)$?*, *Phys. Rev. Lett.* **66** (1991) 1815 [SPIRES]; *The Renormalization group improved Higgs sector of the minimal supersymmetric model*, *Phys. Rev.* **D 48** (1993) 4280 [hep-ph/9307201] [SPIRES];
M. Drees and M.M. Nojiri, *One loop corrections to the Higgs sector in minimal supergravity models*, *Phys. Rev.* **D 45** (1992) 2482 [SPIRES];
J.R. Espinosa and R.-J. Zhang, *MSSM lightest CP-even Higgs boson mass to $O(\alpha_s\ \alpha_t)$: the effective potential approach*, *JHEP* **03** (2000) 026 [hep-ph/9912236] [SPIRES];
M.S. Carena et al., *Reconciling the two-loop diagrammatic and effective field theory computations of the mass of the lightest CP-even Higgs boson in the MSSM*, *Nucl. Phys.* **B 580** (2000) 29 [hep-ph/0001002] [SPIRES].

[60] G.L. Kane, T.T. Wang, B.D. Nelson and L.-T. Wang, *Theoretical implications of the LEP Higgs search*, *Phys. Rev.* **D 71** (2005) 035006 [hep-ph/0407001] [SPIRES];
M. Drees, *A supersymmetric explanation of the excess of Higgs-like events at LEP*, *Phys. Rev.* **D 71** (2005) 115006 [hep-ph/0502075] [SPIRES];
A. Belyaev, Q.-H. Cao, D. Nomura, K. Tobe and C.P. Yuan, *Light MSSM Higgs boson scenario and its test at hadron colliders*, *Phys. Rev. Lett.* **100** (2008) 061801 [hep-ph/0609079] [SPIRES].

[61] S.G. Kim et al., *A solution for little hierarchy problem and $b \to s\gamma$*, *Phys. Rev.* **D 74** (2006) 115016 [hep-ph/0609076] [SPIRES].

[62] M. Asano, S. Matsumoto, M. Senami and H. Sugiyama, *Neutralino dark matter in light Higgs boson scenario*, *Phys. Lett.* **B 663** (2008) 330 [arXiv:0711.3950] [SPIRES].

[63] S.G. Kim, N. Maekawa, K.I. Nagao, K. Sakurai and T. Yoshikawa, *Neutralino dark matter in minimal supersymmetric standard model with natural light Higgs sector*, *Phys. Rev.* **D 78** (2008) 075010 [arXiv:0804.3084] [SPIRES].

[64] W.-S. Hou, *Enhanced charged Higgs boson effects in $B^- \to \tau\bar{\nu}$, $\mu\bar{\nu}$ and $b \to \tau\bar{\nu} + X$*, *Phys. Rev.* **D 48** (1993) 2342 [SPIRES].

JHEP10(2009)005

[65] K.S. Babu and C.F. Kolda, *Higgs mediated $B^0 \to \mu^+\mu^-$ in minimal supersymmetry*, *Phys. Rev. Lett.* **84** (2000) 228 [hep-ph/9909476] [SPIRES].

[66] G. Isidori and P. Paradisi, *Hints of large* $\tan\beta$ *in flavour physics*, *Phys. Lett.* **B 639** (2006) 499 [hep-ph/0605012] [SPIRES];
J.R. Ellis, S. Heinemeyer, K.A. Olive, A.M. Weber and G. Weiglein, *The supersymmetric parameter space in light of B^- physics observables and electroweak precision data*, *JHEP* **08** (2007) 083 [arXiv:0706.0652] [SPIRES];
F. Domingo and U. Ellwanger, *Updated constraints from B physics on the MSSM and the NMSSM*, *JHEP* **12** (2007) 090 [arXiv:0710.3714] [SPIRES].

[67] G. Corcella et al., *HERWIG* 6.5*: an event generator for hadron emission reactions with interfering gluons (including supersymmetric processes)*, *JHEP* **01** (2001) 010 [hep-ph/0011363] [SPIRES].

[68] G. Corcella et al., *HERWIG* 6.5 *release note*, hep-ph/0210213 [SPIRES].

[69] E. Richter-Was, *AcerDET: a particle level fast simulation and reconstruction package for phenomenological studies on high p_T physics at LHC*, hep-ph/0207355 [SPIRES].

[70] B.C. Allanach et al., *The Snowmass points and slopes: benchmarks for SUSY searches*, in *Proceedings of the APS/DPF/DPB summer study on the future of particle physics (Snowmass* 2001*)*, N. Graf ed., *Eur. Phys. J.* **C 25** (2002) 113 [hep-ph/0202233] [SPIRES].

[71] K.-I. Hikasa and M. Kobayashi, *Light scalar top at e^+e^- colliders*, *Phys. Rev.* **D 36** (1987) 724 [SPIRES].

[72] M. Carena, A. Freitas and C.E.M. Wagner, *Light stop searches at the LHC in events with one hard photon or jet and missing energy*, *JHEP* **10** (2008) 109 [arXiv:0808.2298] [SPIRES].

[73] A. Bartl, W. Majerotto and W. Porod, *Squark and gluino decays for large* $\tan\beta$, *Z. Phys.* **C 64** (1994) 499 [*Erratum ibid.* **C 68** (1995) 518] [SPIRES].

[74] U. Chattopadhyay, A. Datta, A. Datta, A. Datta and D.P. Roy, *LHC signature of the minimal SUGRA model with a large soft scalar mass*, *Phys. Lett.* **B 493** (2000) 127 [hep-ph/0008228] [SPIRES].

[75] J. Hisano, K. Kawagoe, R. Kitano and M.M. Nojiri, *Scenery from the top: study of the third generation squarks at CERN LHC*, *Phys. Rev.* **D 66** (2002) 115004 [hep-ph/0204078] [SPIRES];
J. Hisano, K. Kawagoe and M.M. Nojiri, *A detailed study of the gluino decay into the third generation squarks at the CERN LHC*, *Phys. Rev.* **D 68** (2003) 035007 [hep-ph/0304214] [SPIRES].

[76] F. Moortgat and L. Pape, *Hemisphere algorithm for separation of decay chains*, in *CMS physics TDR*, volume II, chapter 13.4, report number CERN-LHCC-2006-021, Cern, Geneva Switzerland (2006), pg. 410 [*J. Phys.* **G 34** (2007) 995] [SPIRES].

[77] S. Matsumoto, M.M. Nojiri and D. Nomura, *Hunting for the top partner in the littlest Higgs model with T-parity at the LHC*, *Phys. Rev.* **D 75** (2007) 055006 [hep-ph/0612249] [SPIRES].

[78] J. Hubisz, J. Lykken, M. Pierini and M. Spiropulu, *Missing energy look-alikes with* $100\,pb^{-1}$ *at the LHC*, *Phys. Rev.* **D 78** (2008) 075008 [arXiv:0805.2398] [SPIRES].

JHEP10(2009)005